42nd Annual Student Design Competition

2024-2025

THE HAWKS

Pioneering Hydrogen Electric VTOL

Sponsored By AIRBUS

Vertical Flight Society

BUP

Signature Page:

Md Khalid Hasan Nabil
Undergrad Student (Team Lead)
nabilhasan01541work@gmail.com

Rasel Khan
Undergrad Student
rasel.khan.ryo@gmail.com

Abu Salehin Ahmed
Undergrad Student
salehin.0987ahmed@gmail.com

Maruf Ahmed
Undergrad Student
marufaerospace@gmail.com

Jubayer Ahmed Sajid
Undergrad Student
sajid.jubayet@gmail.com

Ashab Farhan Anon
Undergrad Student
farhananan1512@gmail.com

Musayeb Hossain Usama
Undergrad Student
mhusama15@gmail.com

Dr. Mohammed Nasir Uddin (MNU)
Professor of Mathematics
Department. of Information and Communication Technology (ICT)
Faculty of Science and Technology
Bangladesh University of Professionals (BUP)
nasiruddin@bup.edu.bd

BANGLADESH UNIVERSITY OF PROFESSIONALS

Department of Information Communication Technology
Mirpur Cantonment, Dhaka-1216, Bangladesh

Permission for Publication:

To the Vertical Flight Society,

The members of the Bangladesh University of Professionals (BUP) Student Design Team in the best new entrant category hereby grant VFS full permission to distribute the enclosed Executive Summary and Final Proposal for the **42nd Annual Student Design Competition 2024–2025** as they see fit.

Thank you,

MD. Khalid Hasan Nabil (Team Lead)
The Hawks Team (Best New Entrant)
Faculty of Science and Technology
Bangladesh University of Professionals (BUP)

Table of Contents

Abstract 1
1. INTRODUCTION 2
1.1 Aircraft design: 2
1.1.1 Guimbal Cabri G2: 420 kg empty, 700 kg max takeoff weight [6] 2
1.1.2 Robinson R22 Beta II: 399 kg empty, 621 kg max [4]. 2
1.2 Propulsion and Power System: 2
1.3 Hydrogen and Propulsion System: 3
1.4 Meeting VFS Competition Requirements: 3
1.5 Modeling and Testing: 3
1.6 Mission Segment 4
1.7 Performance Analysis: 6
1.7.1 CG Location: 9
1.7.2 Hydrogen flow rate and consumption: 9
1.7.3 Vehicle Power Consumption and Aerodynamic Power Consumption: 9
1.7.4 Lift-to-Drag Ratio Formula: 10
2. Design Requirements and Assumptions following RFP 11
2.1 Flight Range of 100 km (about 62.14 mi): 11
2.2 Fitting Rotor Disk Within Dimension of 10 m x 10 m x 4 m: 12
2.3 Stack steady state temperature less than 90°C: 12
2.4 Reach high-voltage (HV) network maximum of 840V: 13
2.5 Specifications of H2 tank as per assumption: 14
2.6 Von Mises Analysis 14
2.7 Tools used: SolidWorks, ANSYS, KeyShot 15
3. Technical Design Description 15
3.1 Airframe and Rotor System: 15
3.1.1 Airframe: 15
3.1.2 Rotor and Rotor Dynamics: 17
3.2 TFCM2-B PEMFC Stack: 21
3.2.1 PEMFC 85 kW System: 23
3.2.2 Fuel Cell Stack Design 23

3.2.3 Fuel Cell Stack 24
3.2.4 Hydrogen Supply Chain 25
3.2.5 Air Supply (Cathode) 25
3.2.6 Water and Humidification 25
3.2.7 Thermal Management 26
3.2.8 Balance of Plant (BoP) and Controls 27
3.2.9 Operating Assumptions 27
3.2.10 Fuel Cell System Modeling and Simulation Results 28
3.3 Low-Temperature Coolant (LTC) System: 31
3.4 High-Temperature Coolant (HTC) System: 31
3.5 Air Intake System: 32
3.6 Cooling System: 32
3.7 Hydrogen (H2) System: 34
3.8 Airflow System: 35
4. Trade Studies and Design Optimization 36
4.1 Mission Range Trade: 36
4.2 Rotor Configuration Trade: 37
4.3 Turbulence Kinetic Energy: 38
4.4 Velocity Streamlines (VS): 39
4.5 Pressure Contour Analysis (PCA): 40
4.6 Design Integration & Flow Optimization: 41
4.7 Quantitative Gains Summary: 41
5.Application and Feasibility Analysis 42
5.1 Affordability Considerations: 42
5.2 Manufacturing and Materials: 43
6. Originality and Aesthetics 45
6.1 Fuel cell and motor placement 45
6.2 Frame design 45
6.3 Cabin (views, instruments,) 46
7. Operational Considerations 47
7.1 Ground handling by flight (H2 refueling, water drainage) 47

7.2 Avionics Systems 47
7.2.1 Control Path: From Pilot to Actuator 49
7.2.2 Power Path: Supplying the System 49
7.2.3 Redundancy: Backup Battery Operation 49
7.2.4 Signal-Power Coordination 49
8. Conclusion 50
References: I
Nomenclature: IV
Table List: VII
Figure List: VIII

Abstract

In response to the 2024–2025 Vertical Flight Society (VFS) Student Design Competition Request for Proposal, this report offers a conceptual re-design of the Cabri G2 and R22 Beta II helicopters, modified to function as a fully hydrogen-electric vertical takeoff and landing (VTOL) aircraft. While preserving mission viability, flight safety, and regulatory feasibility, the design integrates a Proton Exchange Membrane Fuel Cell (PEMFC) propulsion system and high-pressure gaseous hydrogen storage to meet the urgent global demand for zero-emission aviation.

The suggested design is based on an 85 kW PEMFC framework (TFCM2-B), which is taken from the concept of NASA's 2021 PEMFC modeling requirements. By operating below the designated maximum steady-state temperature of 90°C and staying below the 840 V high-voltage constraint, the stack ensures safe, dependable operation within the confines of show innovation. Hydrogen is stored at 700 bars by RFP requirements and industry standards. A 30-kilogram lithium-ion buffer battery is incorporated into the framework to manage top control requirements and guarantee capacity preservation during autorotation and flare maneuvers.

The rotor craft is designed to complete the entire 15-segment "Spearheading Mission" specified in the RFP, which includes a few vertical float fragments, climb and voyage stages, a sharp plummet using autorotation, and a delayed dallying period for natural perception. The by and large setup, based on the Cabri G2 stage, underpins a payload capacity of 185 kg (about 407.85 lb.) and ensures that the airplane fits inside the 10 m × 10 m × 4 m volume limitation (1 pilot, 1 traveler, and baggage). Careful exchange considers that comparing the Cabri G2 to the R22 and the RFP standard affirms its predominance regarding vitality integration potential, autorotation behavior, and auxiliary effortlessness.

Utilizing current-generation certified components and well-known modeling programs like MATLAB, ANSYS, and SolidWorks for execution examination, control calculation, and weight & adjust ponders, the proposed plan gives an innovatively reasonable and temperate arrangement. The report consists of numerous simulations about what we have considered and why the report answers the traditional approach for hydrogen powered vehicles and how they can change the future. This hydrogen-electric VTOL vehicle demonstrates the conceivable outcomes of economical flight without relinquishing execution, security, or reasonableness by distinguishing between development and authenticity. This report fulfills all targets recorded within the RFP, including streamlined execution, framework integration, weight examination, and mission execution. It reflects an intensive and imaginative approach to future rotorcraft planning, proposing a conceivable way toward clean, secure, and effective vertical flight keeping the design more realistic and feasible than the current models out there.

Keywords—Hydrogen-Electric VTOL, Proton Exchange Membrane Fuel Cell (PEMFC), Cabri G2, Autorotation, Vertical Flight Society (VFS), Zero-Emission Aviation, TFCM2-B.

1. INTRODUCTION

Cutting carbon emissions in aviation is essential for a cleaner future. Hydrogen-electric systems are a promising way to achieve this goal [1], [2]. One of the best options for powering aircraft with hydrogen is using proton-exchange membrane fuel cells (PEMFCs), which offer high energy output and only release water as a byproduct. These are especially useful for aircraft that take off and land vertically (VTOL), where regular batteries might not provide enough power [1].

This paper introduces The Hawk, a concept helicopter that runs on hydrogen-electric power. It's based on the well-known R22 Beta II and Cabri G2 helicopter and redesigned to meet the goals of the Vertical Flight Society's (VFS) green aviation competition [5]. The design uses a 85 kW Toyota hydrogen-based engine, a 30 kg battery, and our own rotor system design to show how hydrogen power can work in small helicopters. It looks at flight performance, how hydrogen is stored and used, and how the full system is tested and modeled.

1.1 Aircraft design:

The Hawk is built around the Robinson R22 and Cabri G2—a two-seat helicopter with a simple rotor design that is lightweight and has a built-in safety feature called autorotation [3], [4]. It keeps the original frame and rotor system but uses a new 6.78-meter-wide composite rotor to support a heavier total weight of 624 kg. This extra weight includes hydrogen tanks and electronics. The rotor size increases the air area (about 36.1 m^2), reducing pressure on the blades to around 28 kg/m^2. It also has a payload of 185 kg, which meets the VFS requirement [5].

For comparison, other similar helicopters include:

1.1.1 Guimbal Cabri G2: 420 kg empty, 700 kg max takeoff weight [6].

1.1.2 Robinson R22 Beta II: 399 kg empty, 621 kg max [4].

The Hawk keeps the R22's ability to glide safely if power is lost and fits inside the size limits of 10 m × 10 m × 4 m [5]. It has enough cabin space (at least 1.25 m × 1.5 m) for two people and their gear.

1.2 Propulsion and Power System:

The Hawk is powered by Toyota's TFCM2s-B fuel cell, the same type used in the Toyota Mirai car. It produces 85 kW of electric power and weighs around 109 kg, meeting NASA's target of about 1.1 kW/kg [2], [7]. A 30 kg lithium-ion battery helps provide extra power during takeoff or quick movements, and stores energy when possible.

The fuel cell and battery are connected to a central power system (400–750 V DC), controlled by a built-in power converter. This setup powers the main motor and the aircraft's systems. Toyota's fuel cell includes special features like internal water control, so it doesn't need extra humidifiers [8]. The system also includes:

- A hydrogen pressure regulator
- An electric air compressor to bring in fresh air
- A cooling loop (running at 50–85 °C), using fans and a radiator to get rid of heat

These systems were adapted from car designs and made lighter for aircraft use.

During flight, the fuel cell handles steady power needs (like cruising), while the battery helps with quick bursts. Computer models built in MATLAB/Simulink show that power is shared efficiently between the fuel cell and battery.

1.3 Hydrogen and Propulsion System:

Hydrogen is stored in strong, lightweight tanks (Type IV COPVs) at 700 bars. The amount of hydrogen stored ranges from 4.36 to 15.85 kg, giving 85–300 kWh of usable energy, assuming about 60% fuel cell efficiency. For a typical 100 km mission, about 7–8 kg of hydrogen is enough [2]. The tanks themselves weigh about 15 kg per cubic meter, so 15 kg of hydrogen needs around 90–100 kg of tanks. For our mission, we used 5kg of Hydrogen. Water created by the fuel cell is either used internally or released as vapor, so there's no need for water storage [8]. Air is brought in with a blower and cleaned through a filter. The electric power system is managed by a controller and a 25-kW backup inverter for extra loads. The overall weight and power setup was designed using NASA's tools for electric aircraft [2].

1.4 Meeting VFS Competition Requirements:

- **Range:** The Hawk can fly at least 100 km, more than the required 60 km [5].
- **Safety:** It keeps the R22's autorotation ability, meaning it can glide down safely if power is lost [4].
- **Size:** It fits in the required box of 10 m × 10 m × 4 m [3], [5].
- **Weight:** With a total weight of 624 kg and 185 kg payload, the design meets the required balance between structure and performance [4], [6].
- **Battery:** The 30 kg battery follows the rules and works as part of the hybrid system [5].

1.5 Modeling and Testing:

Several tools were used to test and improve the design:

ANSYS: Used to study stress on the blades and how air flows around the helicopter (drag).

- **MATLAB/Simulink:** Simulated full missions, including fuel use, power sharing, cooling needs, and cruise efficiency.
- **SolidWorks:** Created 3D models to make sure all parts fit inside the aircraft and checked the center of mass.

The Hawk's performance was compared to real helicopters:

- Hover power (66.4kW at 624 kg) matches expected values from the R22. [4].
- Cruise speeds around 148.7 km/h are realistic based on existing data [3], [6].

In short, The Hawk fits within NASA's expected range for hydrogen-powered VTOL aircraft and shows that hydrogen fuel cells can be used safely and effectively in small rotorcraft [2].

1.6 Mission Segment

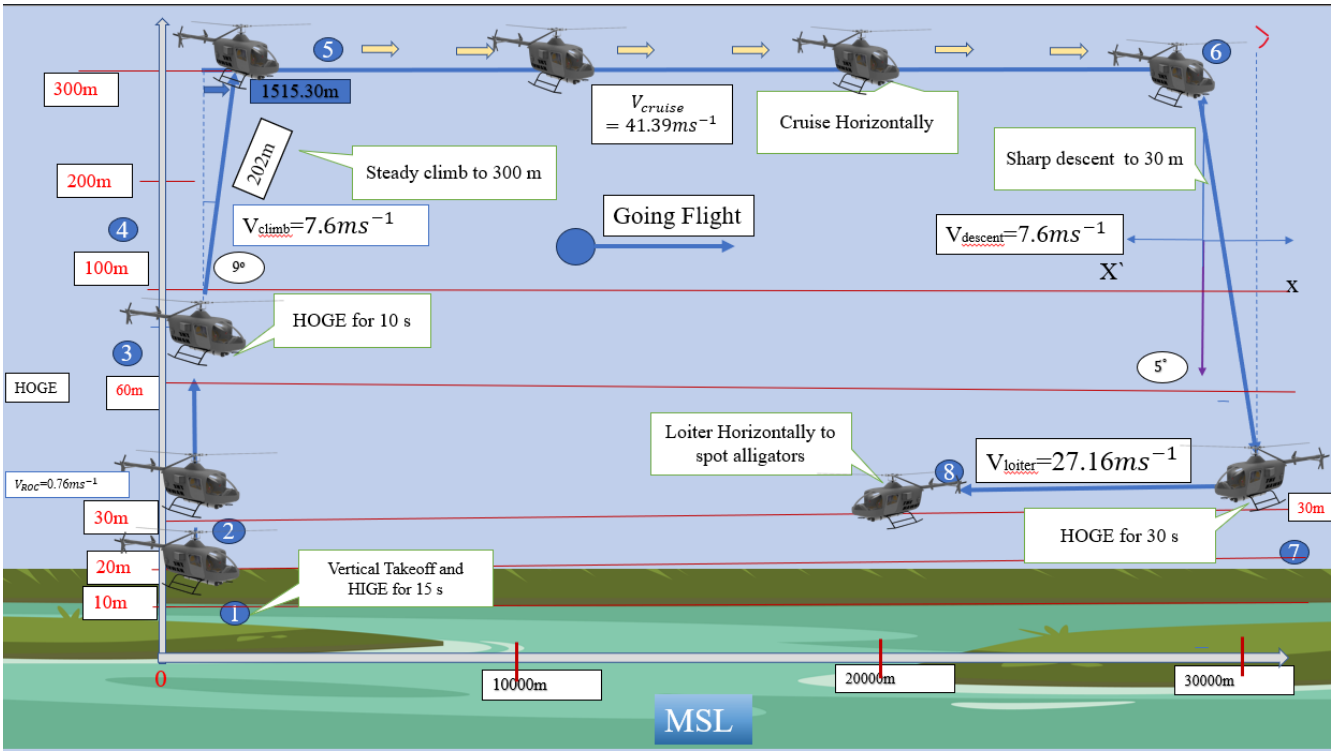

Fig-1.6.i: Going Flight Mission Segment.

The aircraft performs these operations based on the mission segments provided in [5] for going flight: [Fig-1.6.i]

- The aircraft starts at Wright Brothers National Memorial and does normal vertical takeoff to HIGE at MSL.
- The aircraft performs HIGE for 15 s. The position for HIGE is determined to be 10 m above MSL.
- The aircraft climbs 60m from MSL vertically with a velocity of 0.76 m/s.
- The aircraft performs HOGE for 30 s duration at 60 m height.
- At a 9° angle with respect to the ground, the aircraft steadily climbs to 300m, covering a horizontal distance of 1515.30 m. Here the horizontal speed V_{climb} is calculated.
- From this position, the aircraft cruises horizontally with velocity V_{be} traversing 26969.4 m.
- The aircraft descents to 30 m height with velocity $V_{descent}$ = -0.76 m/s through autorotation and with 9° angle.
- The aircraft performs HOGE at 30 m height.
- The aircraft loiters horizontally for 10 seconds to spot the alligators on the river and then returns.

Returning to Wright Brothers National Memorial: [Fig-1.6.ii]

- The aircraft steadily climbs to 300m with 9°angle with respect to the ground again with horizontal velocity $V_{climb.}$
- The aircraft cruises horizontally again with a velocity of V_{be}.
- The aircraft descends to 60 m height with velocity $V_{descent}$
- At 60 m height, it executes HOGE for 10 s for contingency planning.
- It vertically descends with a velocity of 0.76 m/s to the HIGE position.
- It performs HIGE at 10 m above MSL for 15 s.
- The aircraft lands at Wright Brothers National Memorial, right where it started.

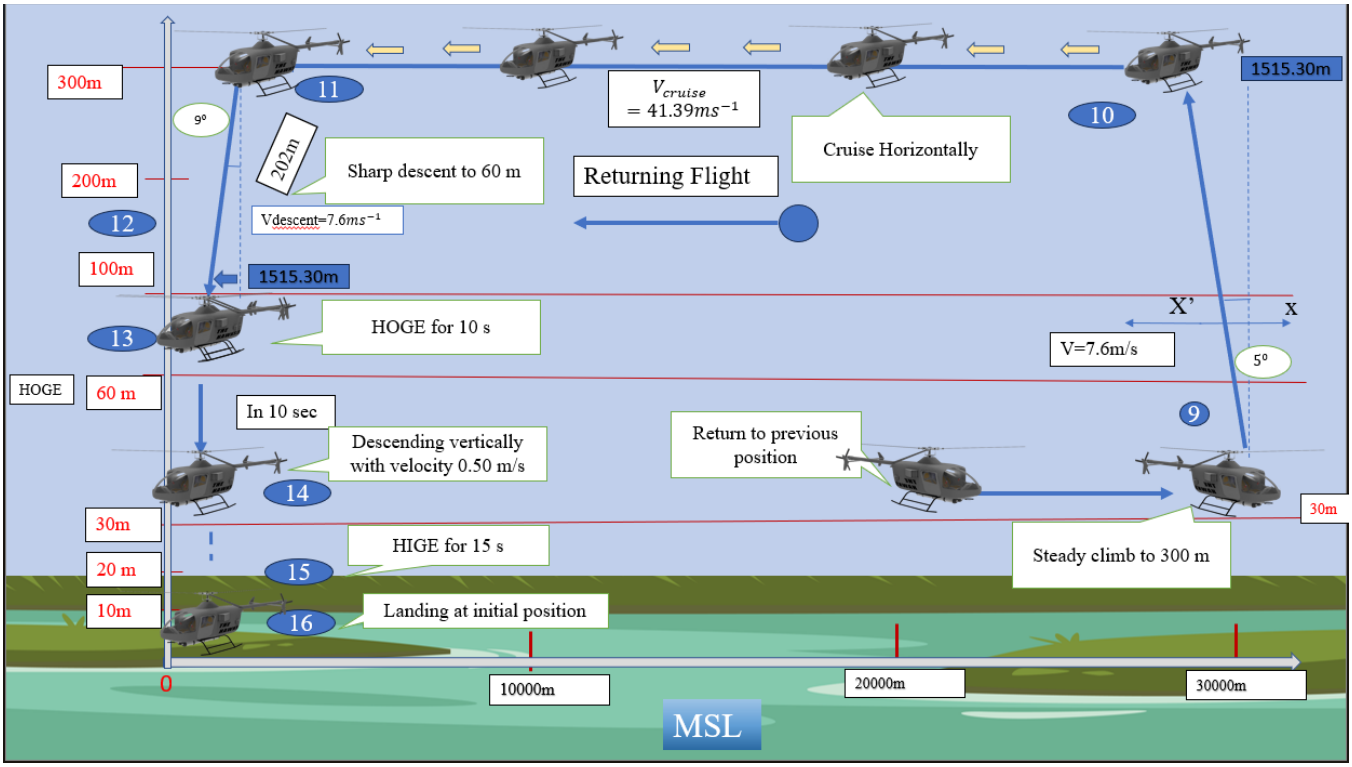

Fig-1.6.ii: Returning Flight Mission Segment.

1.7 Performance Analysis:

We are applying Blade Element Theory to calculate our maximum Thrust, max Power, max Torque .

Our required inputs:

• R: Propeller radius(m)=3.39m • N_b: Number of blades = 3 • ω: Rotational speed(rad/s) =500rpm= $\frac{2\pi n}{t}$ =52.36 rad/s • ρ: Air density (kg/m^3)=1.225 kg/m^3	• V_∞: Axial inflow velocity=(Hover=0) • $c(r)$: Chord distribution=0.18m • $\dot{C}_L$: Lift coefficient=1.46 • C_D: Drag Coefficient=0.023 • r= local radial position of the blade element (m)=400

We used NACA 63015A 2D airfoil for our main rotor. From Xflr5 we got the CL vs α graph which shows us the max CL at 17degree at proper Reynolds number 6.5*e6.

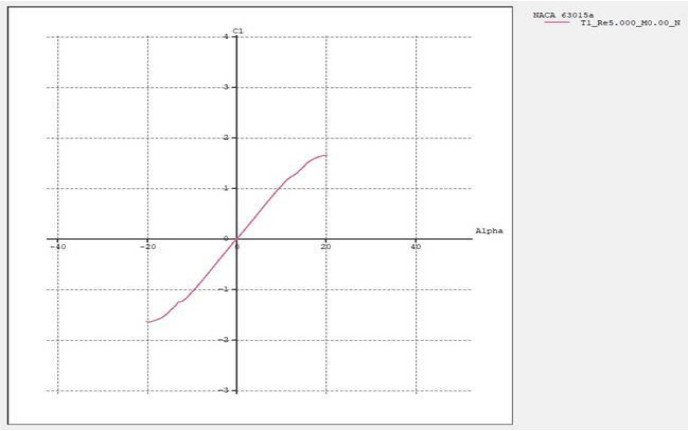

Fig-1.7.i: CL vs Alpha Curve.

So, for our 3D rotor to determine the $C^{l}{}_{3D}$,

α = 17° (highest pitch angle of blade)

Aspect ratio= $\frac{3.39}{0.18} = 18.83$

e= 0.85

Now, Lift curve slope, a = $\frac{5.49}{1+\frac{5.49}{\pi\times0.85\times18.83}} = 4.94$ = 0.086 rad

$C_{L_{3D}=0.086(\alpha-\alpha_{L=0})=1.46}$

Similarly, $C_{D_{3D}=0.023}$

Now, For calculation,

Tangential Velocity (due to rotation), $V_t = \omega . r_i$

Axial Velocity (including induced velocity), $V_a = V_\infty + v_i$

Resultant Relative Velocity , $V_{rel} = \sqrt{V_a^2 + V_t^2}$

Inflow Angle, $\varphi = \tan^{-1}(\frac{V_a}{V_t})$

Differential Lift Force (per element), dL= $\frac{1}{2}\rho V_{rel}.c.C_L.dr$

Differential Drag Force (per element), dD = $\frac{1}{2}\rho V_{rel}^2.c.C_D.dr$

Differential Thrust (Axial Force), dT =$(dL.\cos(\emptyset) - dD.\sin(\emptyset))$

Total Thrust and Torque,

$T_{total} = N_b.\sum dT$

$Q_{total} = N_b.\sum dQ$

Induced Velocity, $v_{new} = \frac{T_{total}}{2\rho A(V_\infty + v_i)}$

Total Power, $P_{total} = Q_{total}.\omega$

So, by iteration in Python, we get our value:

Maximum, T = 17294 N

Torque, τ= 6731.79Nm

Power, P= 35kW.

`blade_element_theory.py` Code reference**:** **https://github.com/not-your-pancake/the_hawk_code.git**

From rfp, $V_{ROC} = 0.76$

Now our requirement to calculate the max Cruise Speed:

$D = \frac{1}{2}\rho V_{cruise}^2 SC_D$

$Cos\theta = \frac{W}{T_{max}} = \frac{624\times9.8}{17294} = 0.354$

$\theta = 69°$

$Sin\theta = \sqrt{1 - (\frac{W}{T_{max}})^2}$

$V_{cruise} = \sqrt{\frac{2T_{max}\sqrt{1-(\frac{W}{T_{max}})^2}}{\rho SC_D}}$ $\sqrt{\frac{2T_{max}Sin\theta}{\rho SC_D}}$ $\sqrt{\frac{2\times17294\times\sin(69°)}{1.225\times36\times0.426}} = 41.39ms/1$

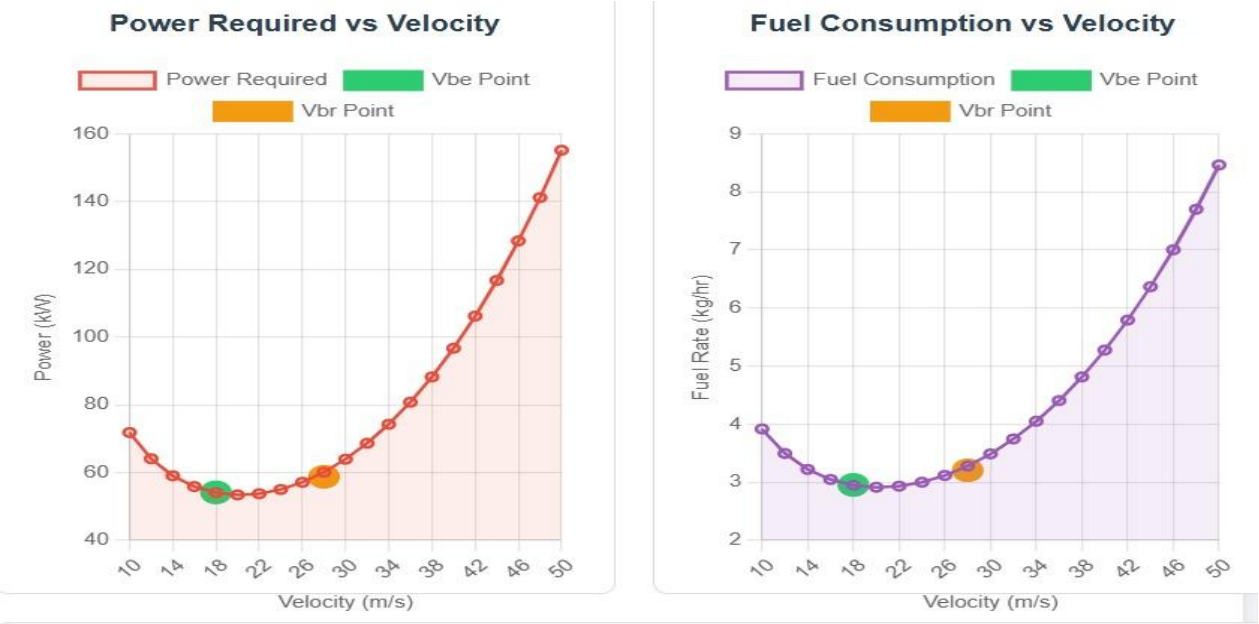

Fig-1.7.ii: Power and Fuel vs Velocity Curve.

From the Power vs Velocity required curve, we find the best endurance speed and best range speed,

$Vbe =$ 17.87m/s, Vbr=27.16m/s

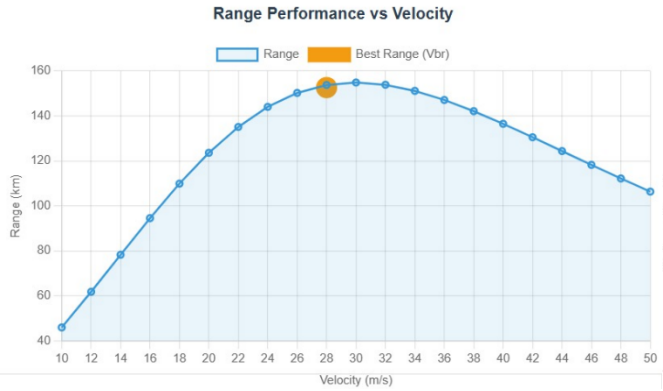

Fig-1.7.iii: Range Performance vs Velocity Curve.

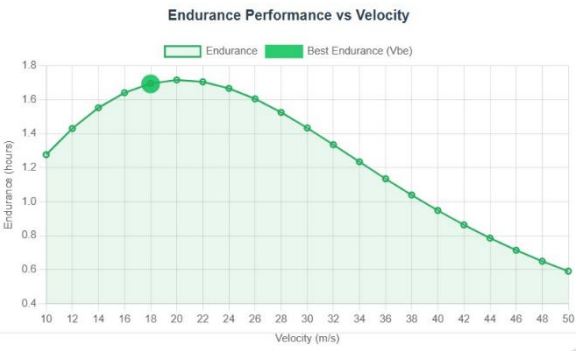

Fig-1.7.iv: Endurance Performance vs Velocity

1.7.1 CG Location:

Our CG is located 1.6m from the nose. The dimensions and the side view of the cg is given below:

Fig-1.7.1.i: Dimension.

Fig-1.7.1.ii: Isometric View.

Fig-1.7.1.iii: Inside View.

1.7.2 Hydrogen flow rate and consumption:

Hydrogen Flow rate and consumption for P_{net}= 85kW PEM fuel cell system:

We know, Lower Heating Valve (LHV) of H_2 =120MJ/kg= 33.33kWh/kg

System efficiency= 50-60%$\approx$55%

So, Hydrogen Consumption Rate, $mH_2 = \frac{P_{net}}{\eta_{sys} \times LHV_{H2}} = \frac{85}{.55 \times 33.33} = 4.637 kg hr^{-1} = 1.29 gs^{-1}$

So, Our total Flight time for 5kg of $H_2 = 1.07hr = 64.7min$

1.7.3 Vehicle Power Consumption and Aerodynamic Power Consumption:

Now to calculate the vehicle power and aerodynamic power for each mission segment:

Hover:

Aerodynamic Power; $P_{hover} = \frac{T^{\frac{3}{2}}}{\sqrt{2\rho A}} = \frac{6115.2^{\frac{3}{2}}}{\sqrt{2 \times 1.225 \times 36.1}} = 50.8kW$

Vehicle Power; $P_{vehicle} = \frac{50.8}{0.9} + 10 = 66.4kW$

Climb Rate:

Aerodynamic Power, $P_{climb} = P_{hover} + W.V_c = 50.8 + (6115.2 \times 7.6) = 46.6kW$

Vehicle Power, $P_{vehicle} = \frac{46.6}{0.9} + 10 = 61.78kW$

Cruise:

Aerodynamic Power, $P_{cruise} = \frac{D.V}{\eta_{prop}} + Rotor\ profile\ loss = \frac{300 \times 41.39}{0.75} + 20 = 16.6kW$

Vehicle Power, $P_{vehicle} = \frac{16.6}{0.9} + 10 = 28.44kW$

Descent:

Aerodynamic Power, $P_{descent} = P_{hover} - W.Vc = |50.8 - (6115.2 \times 7.6)| = 46kW$

Vehicle Power, $P_{vehicle} = \frac{46}{0.9} + 10 = 61.1kW$

Final Hover:

Same as hover power; $P_{hover} = 50.8kW, \quad P_{aerodynamic} = 66.4kW$

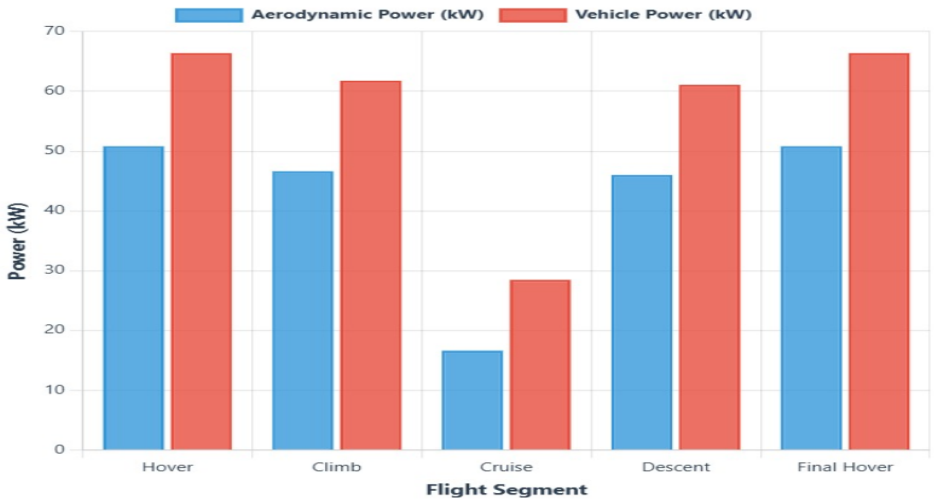

Fig-1.7.3.i: Aerodynamic Power and Vehicle Power Comparison for Each Segment.

Segment	Power level	Demand	Estimated Transmission
Hover	High	High torque demand, motor at near-optimal load	o.91-0.92
Climb	Very High	Peak Power, best motor efficiency range	0.92-0.93
Cruise	Moderate	Low load, inverter/motor may be less efficient	O.90-0.91
Descent	Low to moderate	Lower torque possible reduced motor efficiency	0.89-0.90
Final Hover	High	Same a s initial hover	0.91-0.92

Table- 1.7.3.i: Velocity Transmission Efficiency.

1.7.4 Lift-to-Drag Ratio Formula:

$(L/D)_e = MTOW \cdot g \cdot V\infty / Pshaft, tot$

Where: MTOW = 6115.2 N, g = 9.81 m/s², V∞ = airspeed, Pshaft, tot = total shaft power.

In the graph the best endurance and best range speed are also showed:

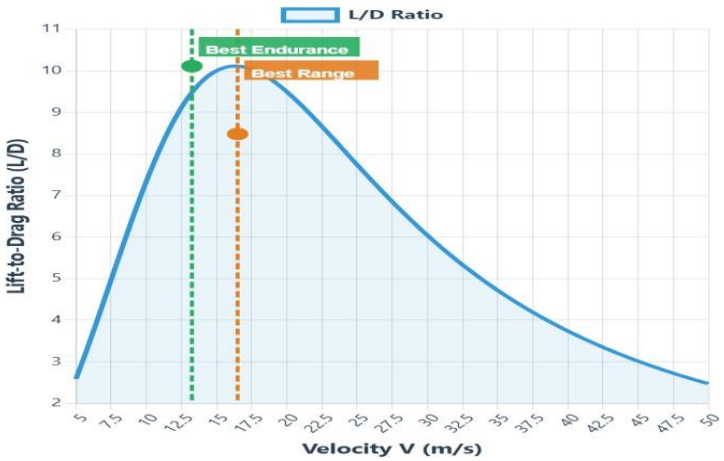

Fig-1.7.4.i: Lift to Drag Ratio vs Velocity.

2. Design Requirements and Assumptions following RFP

General Requirement: One pilot and one passenger to view alligators

The Hawk model is specially designed which is capable of hydrogen propulsion and effective alligator detection in natural areas. Its compact yet robust airframe paired with wide view of canopy ensures excellent aerial visibility, for passengers comfort the interior is designed very well and spacious, also providing a glass view to see the alligators directly underneath the aircraft. The side mounted sensor pods and unobstructed front view, the hawk is capable of detecting alligators under foliage and high tide rivers, providing a reliable surveillance solution for wildlife monitoring as well as tourism and peak adventures keeping environment friendly.

2.1 Flight Range of 100 km (about 62.14 mi):

Our rotorcraft is engineered to achieve a total flight range of approximately 100km (about 62.14 mi) under steady state cruising conditions. This performance mostly depends on the PEM fuel cell stack and high efficiency propulsion system.

The primary power source of our rotorcraft (Toyota Mirai Gen 2 fuel cell stack) delivers up to 185kW peak power and its system efficiency is about 44%. This high efficiency allows energy dense flight operations. Here the net power required would be about 50-55 KW, and output voltage is 650V DC. The 700bar hydrogen tank can take up to 120 L volume space of H2. With the total power of 50-55 KW the downward flight continues up to 1.1-1.2 hours.

So, with a full 5 kg onboard hydrogen load, stable electrical demand and optimized cruise speed, the rotorcraft can maintain energy margin for loiter and emergency hover.

2.2 Fitting Rotor Disk Within Dimension of 10 m x 10 m x 4 m:

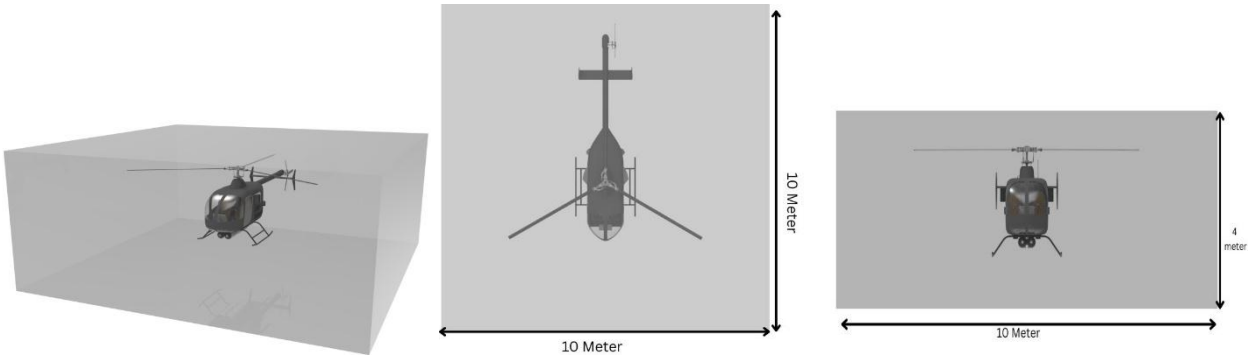

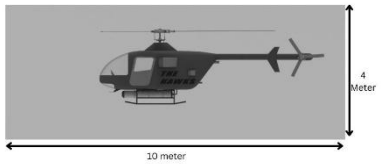

According to the SDC, RFP the Hawk's height is within 4m.

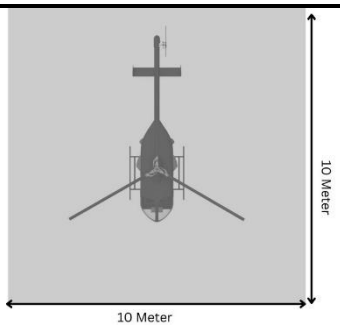

The rotors of the Hawk fit in the 10m x 10m x 4m rectangular prism perfectly.

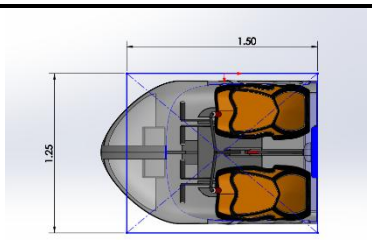

The interior usable cabin floor also meets the 1.25m x 1.5m dimensions perfectly.

Fig- 2.2.i: Examples of Conceptual VTOL Aircraft That Fulfill the Dimensional Requirements.

Our designed model, The Hawk, fulfills all the requirements that were stated by the RFP. The RFP asks us for our model to fit within a cabin space requirement of 10 m x 10 m x 4 m, so we created our model on that basis. For validation, we have attached the necessary dimensions for the cabin space and fitted our model The Hawk within that dimension. Our model fulfills those criteria with a landslide.

2.3 Stack steady state temperature less than 90°C:

The RFP asks us to use an LTC coolant system under 90 degrees centigrade. We have used such, for validation, we used ANSYS fluent to validate our coolant. The simulation revealed a peak system temperature of just 50 degrees centigrade which comes around a maximum at 323 kelvins[9]. It is

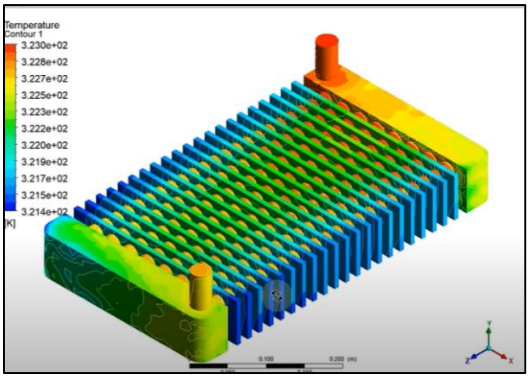

significantly below the threshold limit of 90 degrees centigrade. The radiator performed as expected and overall, the cooling system is highly efficient and fit for use.

Fig-2.3.i: LTC Cooling System Showing That Its Perfectly Functioning Under 90° C.

2.4 Reach high-voltage (HV) network maximum of 840V:

Fig-2.4.i: EMRAX 268 Motor Integration With Main and Tail Rotor.

The EMRAX 268 is a powerful and lightweight electric motor that works well in airplanes that use high-voltage systems, like the Reach system, which goes up to 840 volts. Using high voltage helps the motor work more efficiently and lets it use thinner wires, which makes the whole aircraft lighter and better at saving energy.

This motor can produce a maximum power of 230 kW and run continuously at 100 kW without overheating. It can also create a lot of torque, which is important for taking off and flying.

The EMRAX 268 is great for high-voltage systems because:

- It runs more efficiently, with less energy wasted than heat.
- It supports cooling in different ways with air or liquid depending on how much cooling is needed.
- It can be combined with another one to make even more power if needed.
  It's lightweight (only about 21.4 kg for the air-cooled version), which is important in airplanes.

Because of all these features, the EMRAX 268 is a good choice for new electric aircraft that are designed to use high-voltage systems like Reach's 840V network. It gives strong performance, saves energy, and helps keep the aircraft light.

Electrical	
Maximum Battery Voltage	830 (HV) / 830 (MV) / 340 Vdc (LV)
Peak Power (at 4500 RPM)	210 KW
Continuous power*	Up to 117 KW
Peak torque	500 Nm
Continuous torque*	Up to 250 Nm
Efficiency	92-98%

Table-2.4.i: Electrical Specifications of Motor [13]

2.5 Specifications of H2 tank as per assumption:

The carbon fiber composite cylinder design demonstrates acceptable performance under 700 bar internal pressure loading [10]. The maximum deformation of 163.35 mm is within the expected limits for this class of pressure vessel, and the stress distribution pattern indicates proper load transfer throughout the structure.

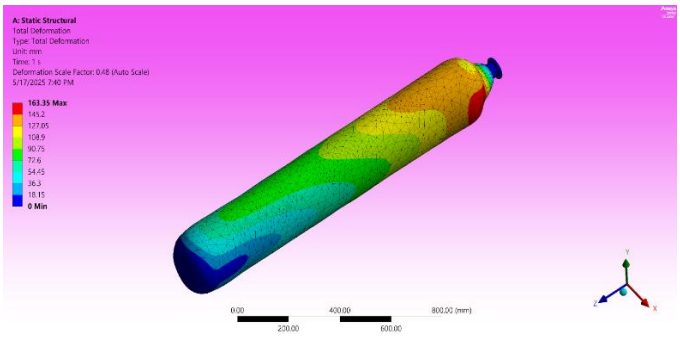

Fig-2.5.i: Total Deformation under pressure

Composite Material Advantage: Carbon fiber composites typically have tensile strengths of 3,500-7,000 MPa [11], significantly higher than traditional pressure vessel materials like steel (400-850 MPa), making them ideal for high-pressure applications. **Safety Margin**: The presence of a Safety Factor calculation in the solution tree suggests the design includes appropriate engineering margins beyond operational requirements.

The carbon fiber composite cylinder design is structurally sound for the intended 700 bar pressure application. The deformation pattern and magnitude are within acceptable limits for this class of pressure vessels. The comprehensive analysis approach, including deformation, stress, fatigue, and safety factor assessments, provides confidence in the design's integrity under the specified operating conditions.

2.6 Von Mises Analysis

Static structural analysis was done to examine the equivalent (von Mises) stress distribution in the carbon fiber composite cylinder under 700 bar internal pressure.

.

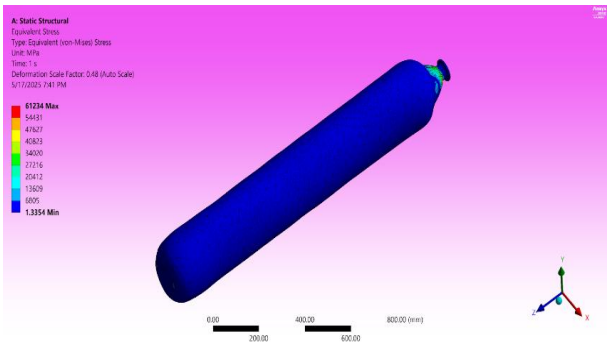

Fig-2.6.i: Von Mises Analysis on Cylinder.

The carbon fiber composite cylinder design for 700 bar internal pressure application demonstrates promising performance characteristics based on comprehensive structural analysis. The deformation behavior is controlled and predictable, while stress distribution is manageable throughout most of the structure with localized concentrations that can be addressed through targeted design refinements. With appropriate safety factors and fatigue considerations included in the analysis process, the design approach is sound and suitable for high-pressure hydrogen storage applications, provided that the identified stress concentration areas are properly addressed in the final design iteration.

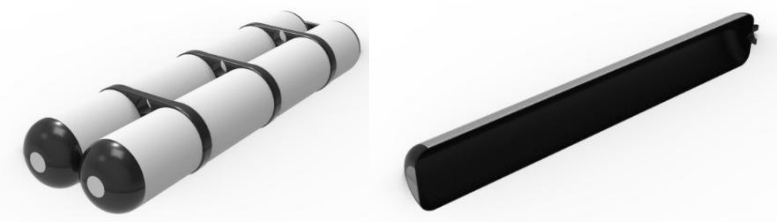

Fig-2.6.ii: (60+60 L) H2 tank and cross section.

2.7 Tools used: **SolidWorks, ANSYS, KeyShot .**

3. Technical Design Description

3.1 Airframe and Rotor System:

3.1.1 Airframe:

Here we created a CAD model of the main frame using SolidWorks. The truss type structure is inspired by endurance off road racing vehicle frames such as trophy trucks, offering lightweight structure with great strength. For frame validity, we used SolidWorks for statics emulation.

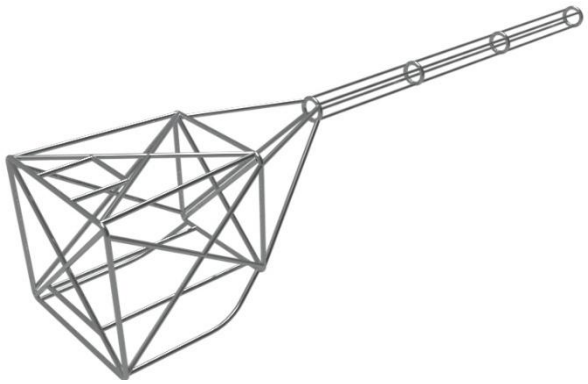

Fig-3.1.1.i: Truss Type Aluminum Tubular Frame

3.1.1.1 Chassis Simulation Analysis Report:

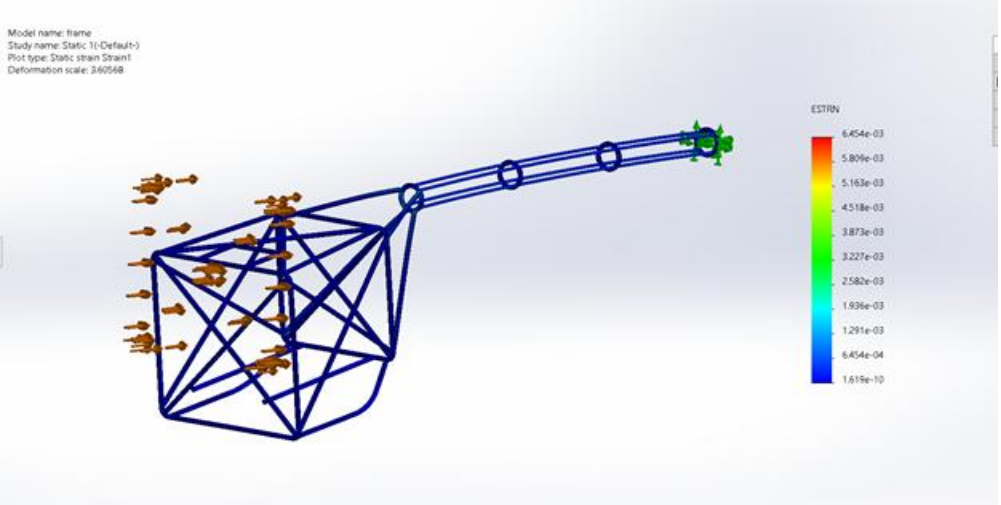

Aluminum 6061-T6 performs exceptionally well under load and proves our structure of the airframe can withstand much greater force during accidents or loads and perform under several loading conditions.

Fig-3.1.1.1.i: Airframe static strain Chassis Simulation

3.1.1.2 Stress Analysis:

The stress distribution analysis reveals the structural response of the aluminum chassis under the applied loading conditions. Critical stress concentrations were observed at the front of the chassis where the load was applied.

Here we used parameters like material Aluminum 6061-T6 which is an excellent heat-treated alloy with good strength to weight ratio, and keeping the rear fixed we applied around 1000 N force. The color gradient from blue (low stress 1.00e-36) to red (high stress 1.19e+02) shows how load transfers through the structure. The simulation was done on SolidWorks due to meshing issues in Ansys, but the results were as expected. Aluminum connection points and areas of geometric transition.

3.1.1.3 Displacement Results:

The displacement analysis shows the deformation pattern of the chassis structure, indicating how the frame responds to the 1000 N loading while constrained at the rear mounting points. With Aluminum 6061-T6 having a yield strength of approximately 276 MPa, the simulation results can be evaluated against this threshold to determine the safety factor and structural adequacy.

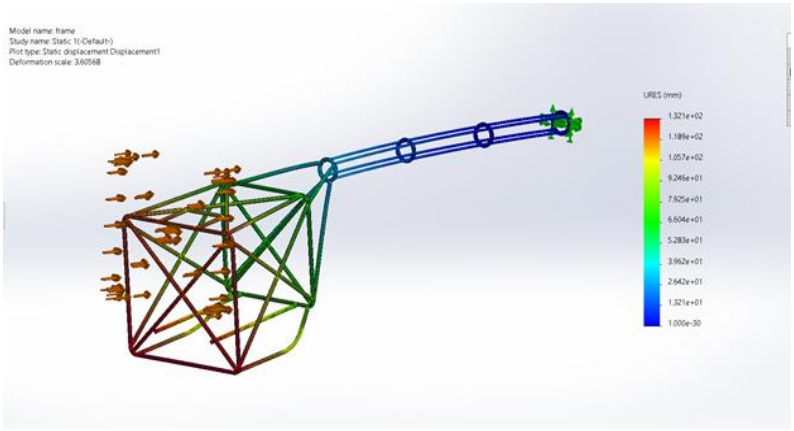

Fig- 3.1.1.3.i: Static Displacement Analysis.

The finite element analysis provides valuable insights into the chassis structural behavior under the specified loading conditions. The results demonstrate the framework's response characteristics and help validate the design's structural integrity.

3.1.2 Rotor and Rotor Dynamics:

3.1.2.1 Rotor type

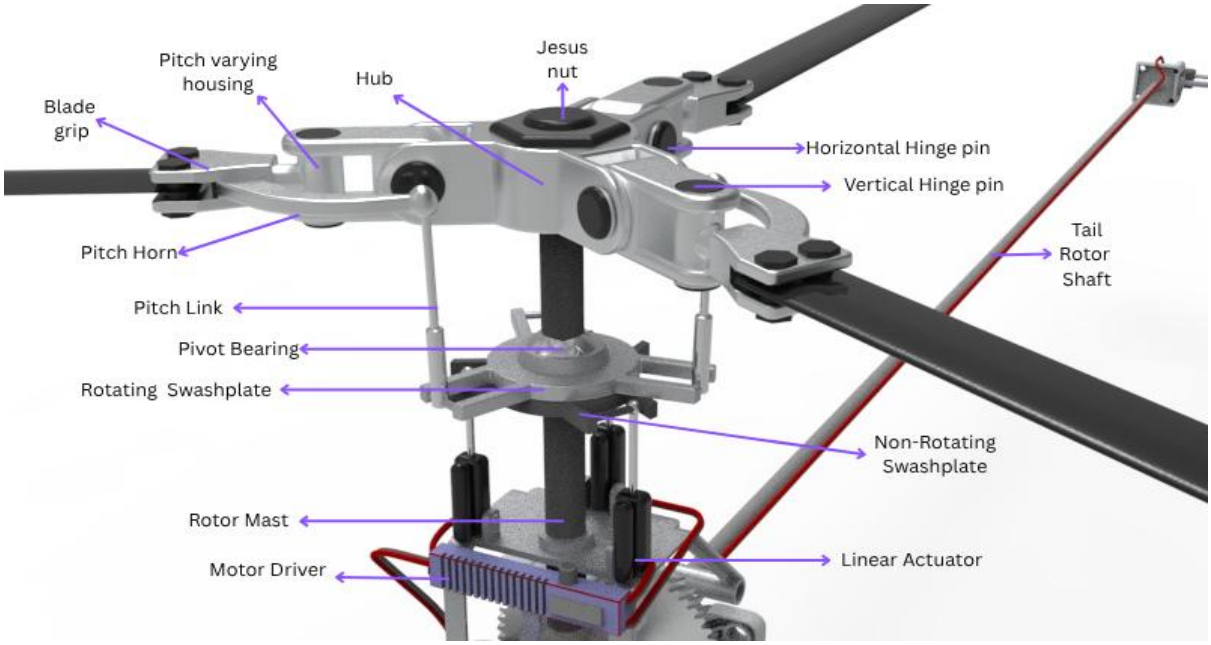

Fig- 3.1.2.1.i: Fully Articulated Main Rotor System

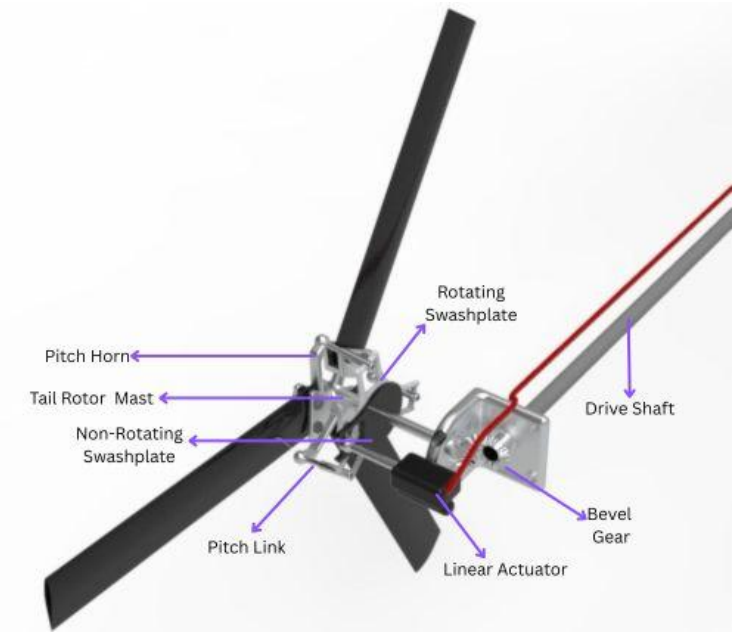

Fig- 3.1.2.1.ii: Tail rotor with actuator.

For the rotor system we used a fully articulated rotor system for our design, the main reasons behind our choice are given as follows:

Stability and Control: Our rotor system is crucial for the independent movement of the system's flapping, feathering, and lead-lag hinges. It ensures stable flight and precise maneuvers, which is ideal for completing tasks like hovering and navigating.
Design Validation: This system has been proven in aviation and is widely used in real helicopters like UH-60 Black Hawk[12]. This is also reliable and easier to model. Also, it ensures more safety for flights.
Load Capacity: The hinges present are robust and capable of handling loads and inertial stresses, handling gusts, and are also very common in competition scenarios.
Simple Control: The swashplate present can provide intuitive pitch control. This suits both manual and automated systems for competition prototypes.
Model Friendly: This system has the adaptability to be suited for small models with easily accessible components. The budget is also less than our competitors'.

3.1.2.2 Control Mechanism:

Fig- 3.1.2.2.i: Flapping

Fig- 3.1.2.2.ii: Lead Lag

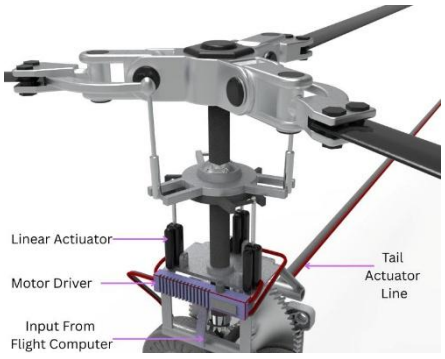

Fig- 3.1.2.2.ii: Control Mechanism

Fig- 3.1.2.2.ii: Pitch

Our fully articulated rotor system helps the Hawks' blades move in three ways: up and down (flapping), back and forth (lead-lag), and twisting (pitching).

- **Flapping (Up and Down Movement):** The **Horizontal Hinge Pin** and **Vertical Hinge Pin** let the blades move up and down. This helps keep the Hawks steady when flying forward by changing how much lift the blades make. The Hub, which is connected to the **Rotor Mast**, holds everything together and lets the blades flap.
- **Lead-Lag (Back and Forth Movement)**: The **Pivot Bearing** lets the blades move a little forward and backward. This stops the blades from getting too much stress as they spin at different speeds. The **Blade Grip** and **Hub** help the blades move this way.
- **Pitching (Twisting the Blades):** The **Pitch Varying Housing** and **Pitch Horn** twist the blades to change their angle. The **Pitch Link** connects the **Pitch Horn** to the **Swashplate** (there are two parts: the Rotating Swashplate and the **Non-Rotating Swashplate**). The **Linear Actuator** moves the swashplate up, down, or tilts it. This changes the blade angle to help the Hawks go up, down, or turn. The **Jesus Nut** keeps the hub tightly connected to the rotor mast, so nothing comes loose. The **Motor Driver** spins the **Rotor Mast**, making the blades turn. The **Tail Rotor Shaft** helps control which way the Hawks go. The swashplate system follows the pilot's controls and moves the blades the right way to fly smoothly.

3.1.2.3 Dimensions and weight:

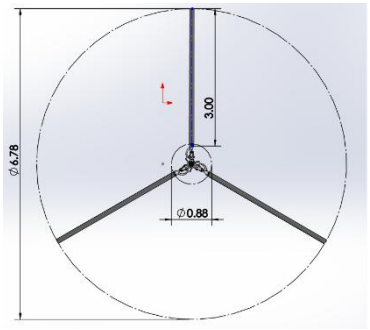

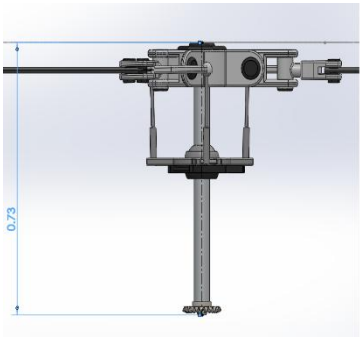

Name	NACA 63-015A AIRFOIL
Chord	180 mm
Radius	0 mm
Origin	0%
Pitch	0°

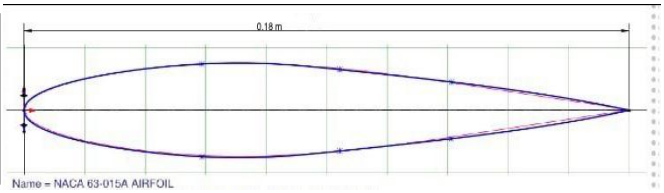

Fig- 3.1.2.3.i: Main rotor system dimension.

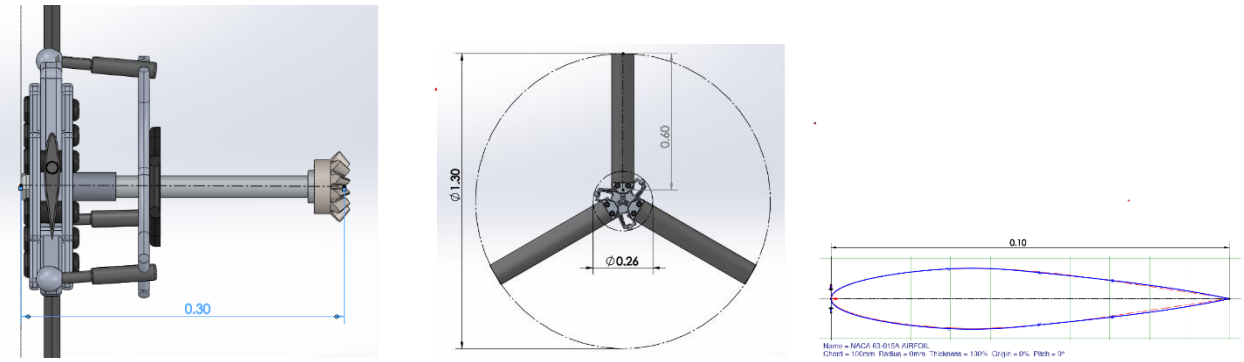

Fig- 3.1.2.3.ii: Tail rotor dimensions.

3.1.2.4 Blade Internal Structure:

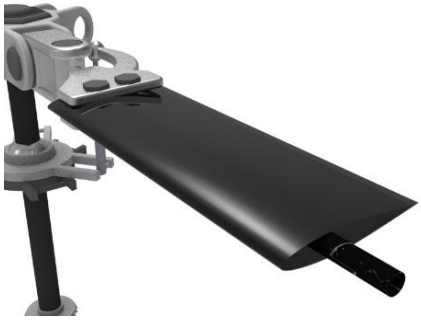

Carbon Fiber Blade is used in the main rotor & tail rotor. Offering weight advantages and strength. The Blade is reinforced with Carbon fiber tube. The 3-meter-long main rotor blade only weighs 3.62 kilograms.

Fig- 3.1.2.4.i: Blade Structure.

3.1.2.5 Reduction Gear Assembly:

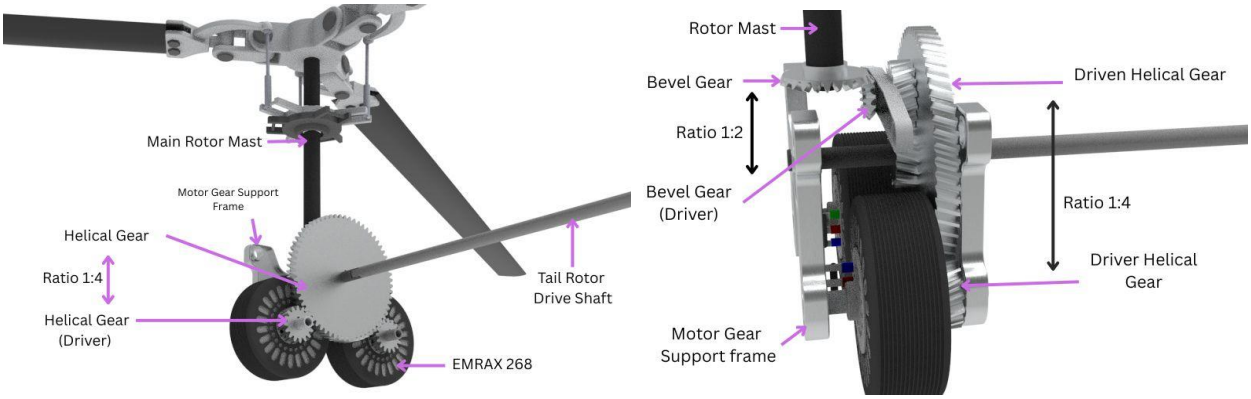

Fig- 3.1.2.5.i: Reduction Gear.

Main motor is connected with helical gear (driver gear). The driver gears drive another helical gear having ratio 1:4. The driven helical gear drives the bevel gear; this bevel gear works as the driver gear for the main rotor mast driven bevel gear. The ratio of bevel gears is 1:2. So the overall gear ratio is 1:8, offering an increase in torque. The single unit of Emrax 268 motor provides continuous torque of 250 Nm. Two motors combinedly to produce 500 Nm of continuous torque. So, the main rotor produces an astonishing 4000 Nm of torque. The high rpm of the motors is reduced to 560 rpm. The rotor gear frame is a CNC cut

aluminum frame which holds the two motors and the whole reduction gear assembly together. This frame also holds the motor and reduction gear together with the main frame. The helical gears of a smooth operation at higher rpm.

3.1.2.6 Mass table:

Component	Main rotor (Kg)	Tail rotor (kg)
Rotor hub	2.27	0.03
Rotor mast	3.36	0.11
Grip & pitch horn	1.02	0.06
Blade	2.13	0.39
Pitch link	0.04	0.01
Swashplate (Rotating)	0.71	0.08
Swashplate(non-rotating)	0.60	0.05

Table- 3.1.2.6.i: Mass table of the main and tail rotor.

3.2 TFCM2-B PEMFC Stack:

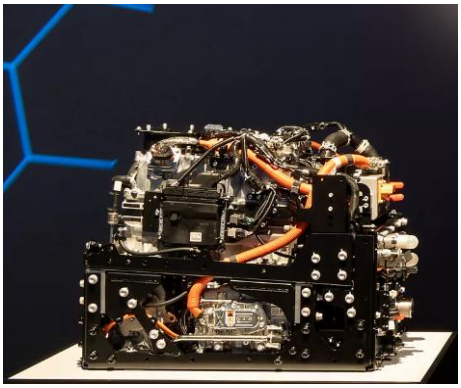

Fig-3.2.i: TFCM2-B [14]

We used this Toyota engine as it supports our sizing and efficiency requirements. We designed our own cad model to visualize all the components. The components that are included in this engine are the LTC pump, water pump, hydrogen pump, air compressor, humidifier, and cooler pump. We also showed the integration of pipe into the different pump in our cad model. The weight estimation is the same as the main model, and we have input this engine into our frame. We couldn't get the full information on this engine from its source, but we tried our best to showcase the design from our point of view.

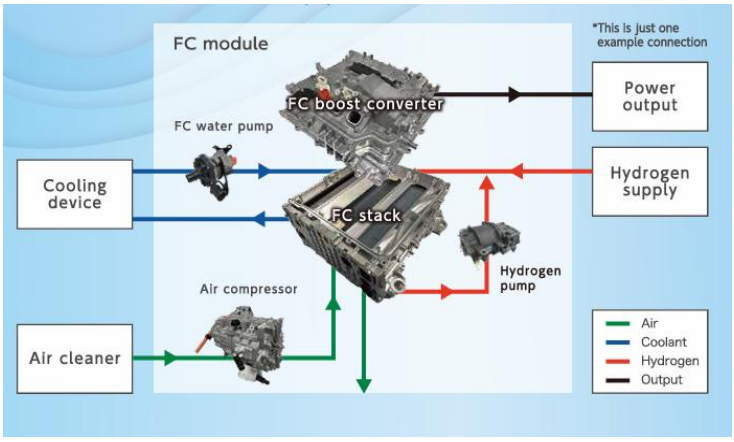

Fig-3.2.iii: FC module [14]

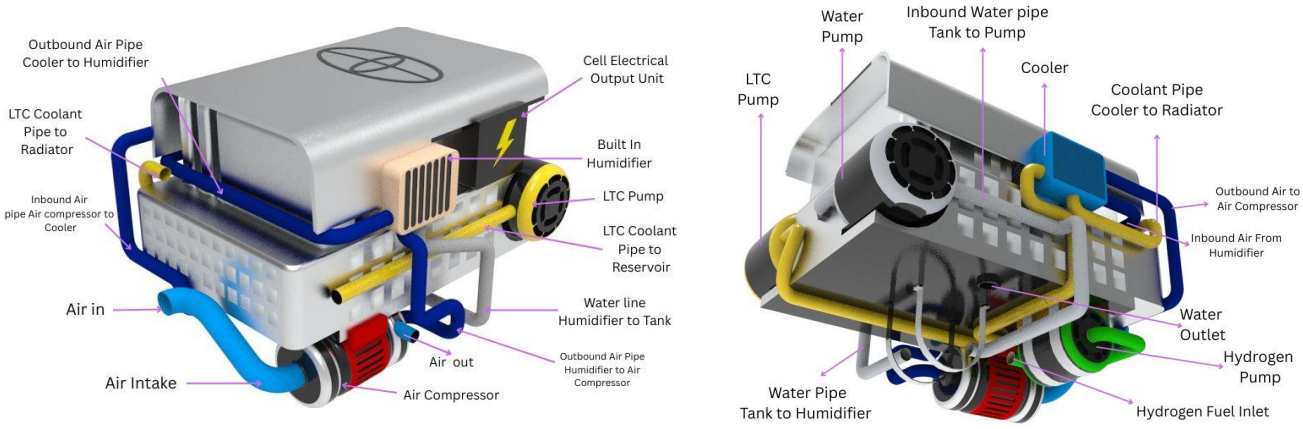

Fig-3.2.ii: Toyota TFC-M2B Fuel Cell System CAD Model

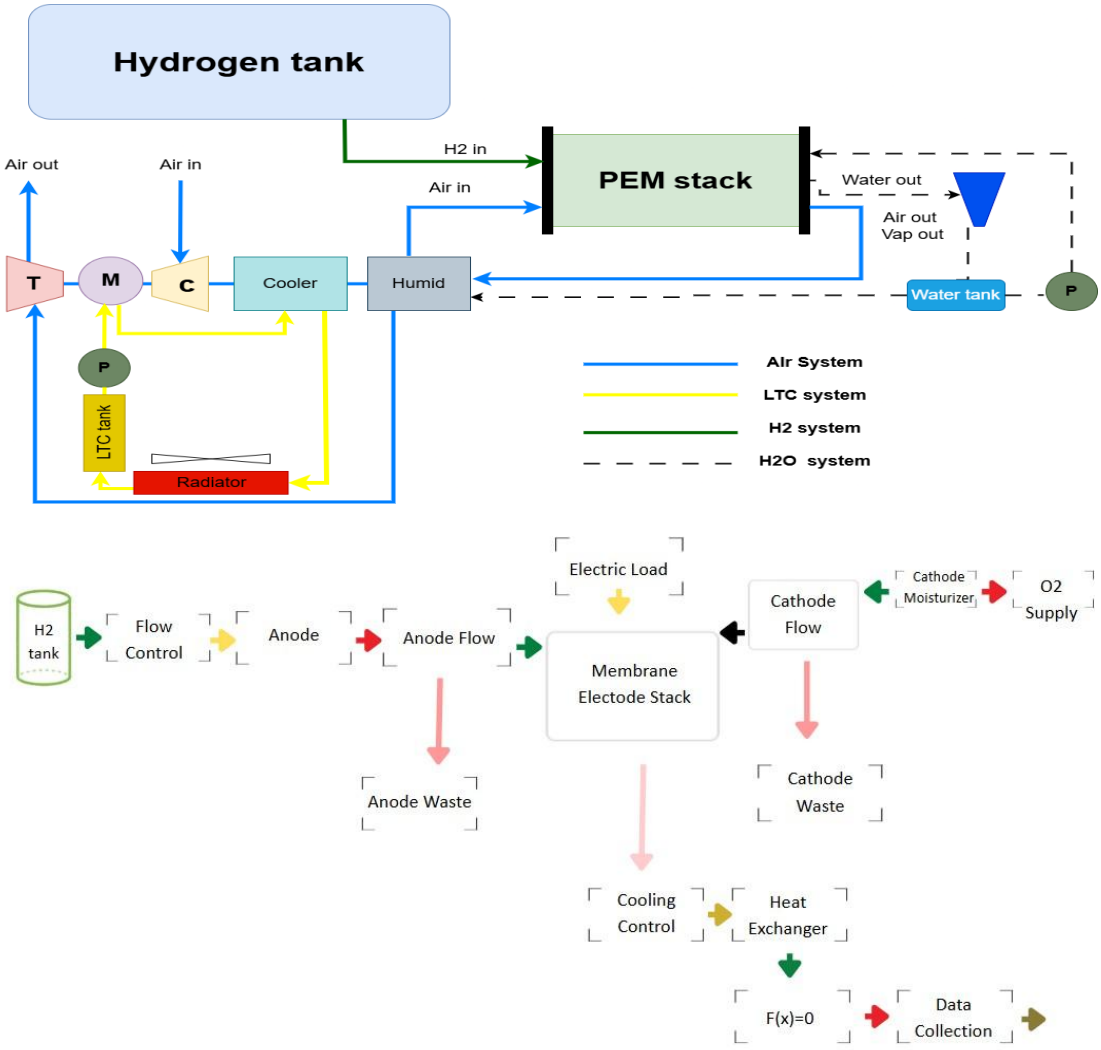

Fig-3.2.v: PEMFC architecture.[2]

3.2.1 PEMFC 85 kW System:

The PEM fuel cell (PEMFC) system is based on a high-pressure (700 bar) hydrogen storage and a 400-cell PEM stack (285 cm² per cell) producing 85 kW peak power output [15] Hydrogen is stored in two Type IV [16] composite tanks (polymer liner with carbon-fiber overwrap) at 700 bars. A pressure regulator and valve chain reduce the pressure to a few bars and send this to the fuel cell anode and controls flow. From calculation we are using 5kg of Hydrogen gas.

Subsystem	Parameter	Value
Fuel Tank	Chamber Volume	120 liters
	Cross-Sectional Area	0.038 m²
Hydrogen Pipe	Length	55 cm
	Cross-Sectional Area	0.0007069 m²
Fuel Cell Stack	Number of Cells	400
	Cell Area	285 cm² (0.028 m²)
	Operating Temperature	50 °C
Oxygen Supply	Pipe Length	85 cm
	Cross-Sectional Area	0.0007069 m²
Coolant Channel	Pipe Length	45 cm
	Cross-Sectional Area	7.06858 cm² (0.000706858 m²)
Coolant Tank	Cross-Sectional Area	0.0225 m²
Radiator	Pipe Length	400 cm
	Cross-Sectional Area	0.7854 cm² (0.00007854 m²)
Coolant Return Path	Pipe Length	50 cm
	Cross-Sectional Area	7.06858 cm² (0.000706858 m²)

Table- 3.2.1.i: For 5kg of Hydrogen Tank.

3.2.2 Fuel Cell Stack Design

The stack consists of 400 cells in series (≈260 V at rated current), each 285 cm² active area. It operates at 50° Celsius. The anode reaction is:

$H_2 \rightarrow 2H^+ + 2e^-$ (oxidation); cathode reaction: $\frac{1}{2} O_2 + 2H^+ + 2e^- \rightarrow H_2O$ (reduction)

overall reaction: $H_2 + \frac{1}{2}O_2 \rightarrow H_2O$ [2] [17]

Each cell produces around 0.6–0.7 V underload. All 400 cells produce 240–285 V stack voltage at 85 kW[18] Most PEM cells peak at 0.4–0.8 W/cm² **[19]**, achieved near 0.6–1.2 A/cm². Operating at a lower current density (≈0.6–0.8 A/cm²) balances efficiency and weight, giving roughly 85 kW with each cell at ~0.65–0.7 V. The stack is designed for high output density (DOE fuel cell targets) **[19]**. Platinum catalysts on carbon binders are used in both electrodes; the membrane is a perfluoro sulfonic acid (Nafion-type) polymer.

Stack performance is determined by polarization losses and hydrogen/air flow rates. Cell efficiency (voltage/Eh) decreases at high current due to activation and ohmic losses[19]. The net system efficiency (net electrical power vs. hydrogen energy) is assumed to be ~50–60% (≈0.86–0.90 gross-to-net ratio for BOP losses. Balance-of-plant (BOP) parasitic loads (compressor, pumps) consume ≈10–15% of gross power. The stack design point targets a balance between high power density and acceptable efficiency.

3.2.3 Fuel Cell Stack

The PEMFC stack used in The Hawk is modeled after the TFCM2-B (Toyota Fuel Cell Module 2 - B), a 120 kW-class commercial fuel cell module which is adapted for aerospace integration. The stack is designed as a multi-cell electrochemical reactor, where each cell contributes a small voltage and current, and their series-parallel combination delivers high total power.

Parameter	Value
Fuel Cell Type	PEMFC (Proton Exchange Membrane Fuel Cell)
Number of Cells	400
Active Area per Cell	285 cm²
Total Stack Power	120 kW (nominal)
Nominal Stack Voltage	600 V
Operating Voltage Range	450–650 V
Nominal Current Output	~200 A
Stack Operating Temp	50°C
Stack Cooling	Liquid loop with radiator and thermal mass
Voltage Behavior	Decreases with increasing current (as shown in V-I curve)
Stack Integration	Located in the forward fuselage

Table- 3.2.3.i: Key Fuel Cell Stack Parameters

The MEA (Membrane Electrode Assembly) comprises the electrochemical heart of each cell, where:

- Hydrogen enters the anode channel, releasing electrons.
- Oxygen enters the cathode channel and combines with protons and electrons to form water.

The system requires humidification, cooling, and flow control to maintain efficiency and membrane health.

3.2.4 Hydrogen Supply Chain

High-pressure hydrogen from the tanks passes through a regulator and filters into the anode manifold. Hydrogen fuel cell operation can tolerate low impurities, so a demister filter is included. A pressure relief valve and shutoff valve are safety requirements. In steady operation, anode pressure is set a bit higher than cathode pressure (e.g. ~2–3 bar) to prevent air access. Simultaneously, H_2 is fed in slight excess (e.g. 1.2–1.5× theoretical) to ensure full utilization without fuel starvation [19]. Unused H_2 can be released or recirculated. But for simplicity and less weight, excess flow is vented to the atmosphere.

Two Type IV tanks (120L total) are used which together contain 5kg of hydrogen fuel. DOE data indicate a 5–6 kg/700 bar tank system (~single 2.5 kg usable H_2) has 20 kg mass. So, 20 kg tank mass is expected to be 5 kg H_2. The tanks are connected with high-pressure tubing to a multi-stage regulator, which decreases the pressure down to the stack pressure.

3.2.5 Air Supply (Cathode)

Intake air enters through the U-shaped air intake system. Built in centrifugal air compressor takes in the air and sends the air to the cathode via built in cooler & humidifier. The compressor pressurizes air to a bit above stack pressure (needed oxygen partial pressure). Air stoichiometry is often 2 to 3 times high because only ~21% of air is O_2 and to aid cooling. Typical cell uses ~2–2.5× stoichiometry on oxygen, so total air flow ~10–15 kg/min at 85 kW. Air at high temperature must be cooled before entering the cathode. A low-temperature cooler is used to cool compressed air. The air passes through built in humidifier and the stream passes through a filter to remove liquid or particles.

In the cathode, nitrogen and other inert gases enter without reaction, but they dilute oxygen. For each mole of H_2, 0.5 mol O_2 is consumed. O_2 and H_2 flows are coupled by reaction stoichiometry. Pressure drop in the stack (flow channels) is maintained modestly (≈20–50 kPa [20] to limit compressor work. When the compressor spins faster, excess power recovery is considered, but in this small sized system the power consumed by the built-in compressor is a parasitic load (~8–10 kW).

3.2.6 Water and Humidification

Water management is handled internally, meaning there are no separate humidifier units involved. The electrochemical reaction at the cathode produces H_2O, whether in liquid or vapor form, and water moves through the membrane thanks to electro-osmotic drag and diffusion. Protons that migrate through the polymer membrane help carry water molecules from the anode to the cathode (this is the electro-osmotic drag), while a concentration gradient encourages water to back diffuse from the cathode to the anode. In a steady state, these processes work together to keep the membrane hydrated. If there's too much humidity,

it can flood the pores. So too little humidity can dry out the membrane and increase resistance. Excess water is collected in the water tank (4L) and sent to the built-in humidifier. To avoid drying out of the membranes, water is collected from the tank and sent to the membrane. The design's operating temperature of 50 °C keeps the vapor pressure at a moderate level, which helps with self-humidification.

Internally, a small pump and water separator gather any liquid water at the cathode outlet; a portion is reserved in the tank and sent to the humidifier. While most of the product water exists as vapor with the exhaust. A humidity sensor can be placed in the stack outlets to ensure that hydration remains balanced. NASA guidelines stress that maintaining balanced humidification is crucial; having too little water in the membrane can lead to high ionic resistance [22]. In our low-temperature design, we rely solely on the flux of product water for humidification (assuming there's enough back-diffusion) without needing external pumps.

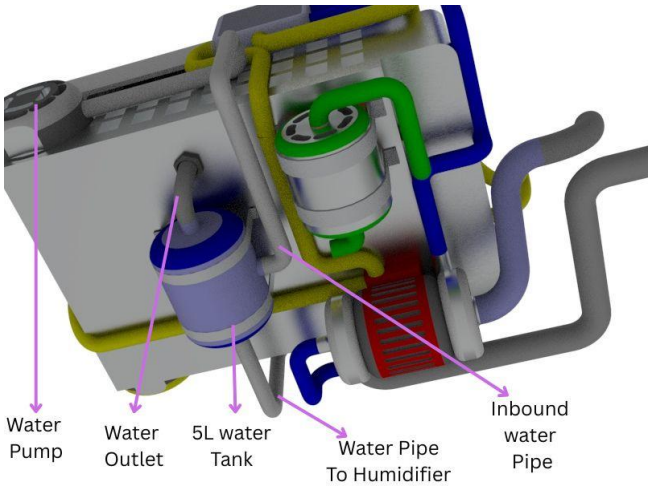

Fig- 3.2.6.1: Humidification and Water Management System CAD model.

3.2.7 Thermal Management

The stack is kept cool by a single low-temperature coolant loop (LTC) that operates at around 40–50 °C. This coolant, a mix of water and glycol, flows through channels or plates built into the stack to effectively remove heat. With an electric output of 85 kW and an efficiency of about 50–60%, we need to get rid of roughly 40–50 kW of waste heat. Since the stack runs at a relatively low temperature, the temperature difference (ΔT) to the surrounding air is minimal, which means we need a large radiator surface area. To handle this heat dissipation, a fan-driven finned crossflow radiator is mounted above the fuel cell. Radiators can add significant weight, which is a crucial factor in our design; therefore, we plan for a lightweight Aluminum finned radiator that can handle around 50 kW during cruise, including a safety margin. Thermal control valves are in place to manage the coolant flow and keep the stack temperature around 50 °C.

The coolant pump and radiator fan are part of the balance of plant (BOP). We consider the coolant pressure drop in the stack and piping when sizing the pump. The loop also includes a reservoir and a thermostat. Since we're only using a low-temperature loop, the coolant exiting the stack is expected to be close to 60 °C, allowing the radiator outlet to reach near ambient temperatures even on hot days. There's no need for a separate high-temperature loop unless other vehicle systems require higher temperatures.

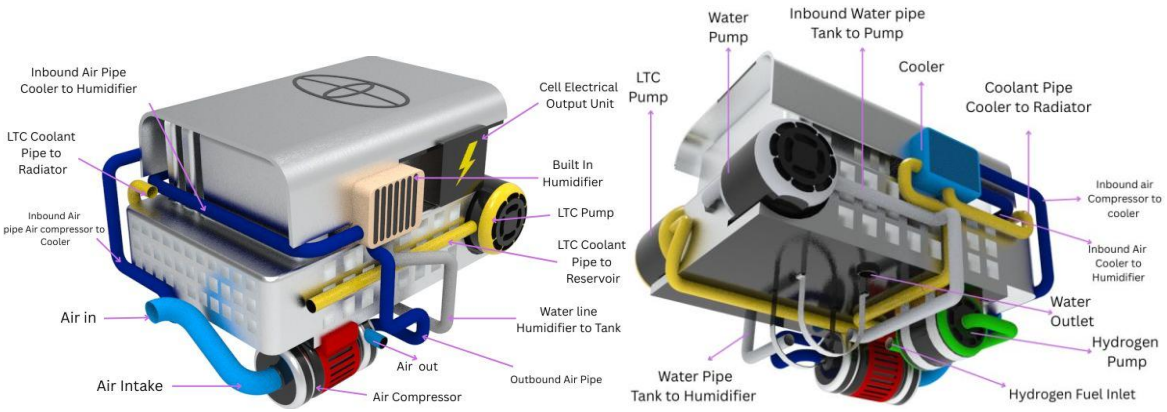

Fig- 3.2.7.i: Cooling System, Air Flow and Fuel Low Integration in The Fuel Cell (CAD model)

3.2.8 Balance of Plant (BoP) and Controls

The BoP includes all components outside the stack. Key elements are:

- Hydrogen supply: pressure regulator, hydrogen pump, and hydrogen pressure sensor for safety.
- Air system: U shaped air intake, air inlet filter, centrifugal air compressor, cooler, and pressure/flow sensors.
- Thermal: coolant pump, heat exchanger (radiator), reservoir, and temperature sensors.
- Water/waste: liquid water separator, drain valve, and optional small water pump (for any recirculation).
- Electrical: DC/DC converter and controls to manage stack voltage/current, instrumentation for stack voltage, current, and individual cell monitoring if used.

These BoP subsystems add parasitic loads and weight. Typical weight fractions (NASA data) allocate ~10–15% of subsystem weight to regulators/valves, filters, plumbing (tubing, fittings), and power components (pumps, motors). For example, regulators and valves control flows; filters remove moisture/debris; pumps and fans move fluids; wiring and controls complete the system.

3.2.9 Operating Assumptions

The stack is rated at 85 kW net. We estimate that there's an operating pressure drop of about 30 kPa across each cell, with leakage being negligible. The ambient intake air, whether at sea level or at a lower pressure due to altitude, gets compressed to the stack pressure. Under design load, the cell voltage is around 0.65 to 0.7 V (which translates to 85 kW/260 V, or roughly 327 A), leading to a cell efficiency of about 55 to 60%. When we look at the net system efficiency—comparing the electrical energy output to the hydrogen's lower heating value—it sits at around 50%, meaning hydrogen consumption is approximately 1.7 g/kWh. NASA's eVTOL fuel cell model aims for a net power fraction of about 0.86 to 0.90, indicating that 10 to 15% of the gross power is used for balance of plant (BOP). As we climb to higher altitudes, cooling and air compression become trickier, so our estimates factor in a slight altitude penalty of less than 5% power loss for every 3000 m.

3.2.10 Fuel Cell System Modeling and Simulation Results

To assess how practical a hydrogen-electric propulsion system would be for The Hawk, we created a detailed simulation using Simulink. Our aim was to mimic the real-world behavior of a power delivery system as it deals with varying electrical loads during different phases of a VTOL mission, including hover, climb, cruise, and descent.

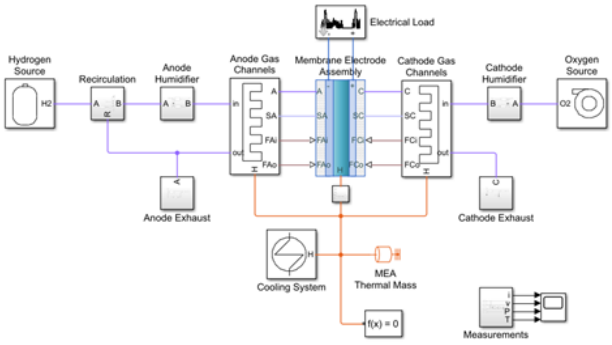

3.2.10.1 System Architecture and Design Rationale

The Simulink model represents a complete electrochemical system that takes in hydrogen and oxygen and converts them into power and thermal energy. As illustrated in [Fig- 3.2.10.1.i], the design is modular and features several essential subsystems:

Fig- 3.2.10.1.i: Architecture and Design Rationale

Hydrogen Fuel Subsystem

- Hydrogen Source supplies high-pressure H_2 to the system.
- A Recirculation loop and Anode Humidifier ensure reactant moisture stability.
- Hydrogen passes through the Anode Gas Channels also distributes it uniformly to the Membrane Electrode Assembly (MEA).

Oxygen Subsystem

- Oxygen Source is humidified before reaching the Cathode Gas Channels.
- Proper humidification is critical for maintaining membrane conductivity in PEMFCs.

Electrochemical Core – MEA

- The MEA comprises 400 cells, each with a 285 cm^2 active area, providing a large reactive surface for proton exchange.
- The stack is configured to produce high-voltage output while minimizing activation and ohmic losses.
- This component converts chemical energy into electrical and thermal energy, forming the core of the propulsion powertrain.

Cooling and Thermal Regulation

- The Cooling Loop includes a coolant pump, radiator (400 cm pipe), and coolant tank.
- The Thermal Mass Block simulates the heat absorption of the stack and surrounding structure.

- We designed the system to regulate stack temperature at 50°C, which is within the operational range defined by the PEMFC manufacturer and consistent with Datta's validation benchmark.

Electrical Output

- The electrical output is delivered to a simulated variable load that replicates real-time demand conditions.
- A Measurement Block tracks voltage, current, power, and temperature continuously.

Design Justification

This system layout is designed to show how PEMFCs are integrated into rotorcraft applications. By recirculating hydrogen, we boost its utilization, while humidification plays a key role in enhancing efficiency. Modular cooling is also a game-changer, ensuring thermal stability—essential for maintaining performance throughout various mission phases. The design features a large stack area and low-resistance flow channels, reflecting a practical approach that strikes a balance between delivering high power output and keeping the system compact.

3.2.10.2 Simulation Inputs and Parameters

All system parameters were based on the baseline architecture from Datta's PEMFC rotorcraft framework, with the following customized values for the Hawk:

Parameter	Value
Number of Cells in Stack	400
Active Area per Cell	280 cm^2
Fuel Tank Volume	1114 L
Hydrogen Pipe Length	55 cm
Pipe Cross-sectional Area	0.0007069 m^2
Oxygen Pipe Length	80 cm
Coolant Channel Length	50 cm
Coolant Channel Area	7.06858 cm^2
Radiator Pipe Length	400 cm
Coolant Tank Area	0.0225 m^2
Stack Operating Temperature Setpoint	50 °C

Table- 3.2.10.2: Simulation Inputs and Parameters

These parameters were selected to provide realistic fluid dynamics and thermal behavior based on known PEMFC propulsion applications.

3.2.10.3 Simulation Output and Analysis

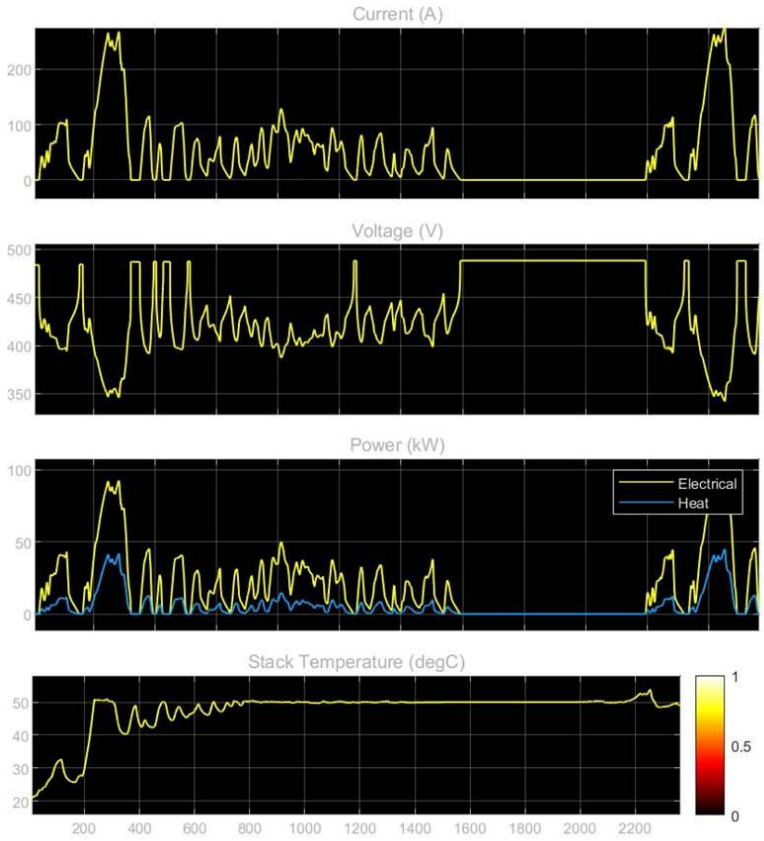

Fig- 3.2.10.3.i: Simulation output

The system was simulated over a 2500-second time window to reflect varying mission loads. The results are visualized in Fig. 2 and described below:

Current (A): The varied a lot which changed with propulsion power. We noticed a sharp rise in power around 200. Those indicate the peak load moments necessary during takeoff.

Voltage (V): As the current increased, the voltage in the stack dropped but was very minimal. This is due to transport losses in PEMFCs. The mission always had a steady flow between 400 to 500 voltages; this meant the design was solid and effective. Occasionally the voltage drops, which is a very realistic response to transient loading.

Power Output (kW): The power output peaked at around 95 to 100 kW; this suits perfectly with smooth cruising and climbing. The thermal power at the same time rises and indicates the heat produced during the energy conversion state. Overall, the system efficiency is naturally 60%, which is normal for a PEMFC system.

Stack Temperature (°C): The stack hits the temperature of 50 degrees centigrade and remains steady throughout the mission. This means that the radiator, coolant, and thermal model work together well. It keeps the temperature in check.

3.3 Low-Temperature Coolant (LTC) System:

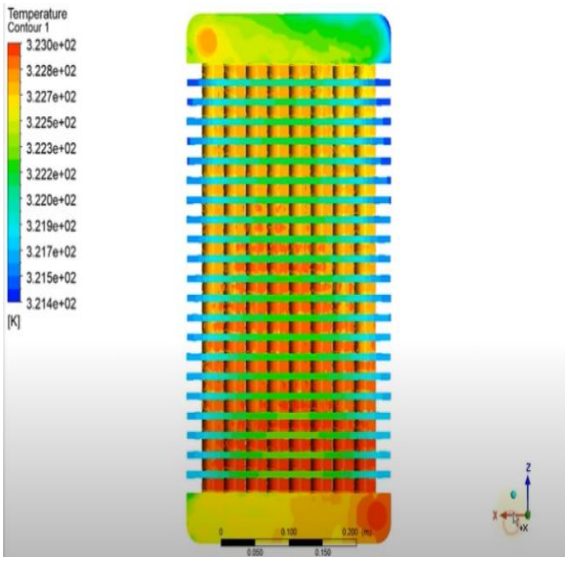

Fig-3.3.i: LTC System

The whole study was done to focus on simulating and validating a liquid cooling system for the PEM fuel cell which is integrated in The Hawk. The mission was to keep the stack temperature below 90 degrees centigrade to ensure operational efficiency. The validation was done on Ansys Fluent; we modeled the system maintaining a heat load that ranges from 50 kw to 70 kw, using a water-glycol coolant mixture. It enters the system at 40 degrees centigrade at 0.01 m3/s. The radiator was kept fixed at 0.4 × 0.28 × 0.05 m exposed to an ambient temperature of 25°C and constructed from aluminum for its high thermal conductivity.

The turbulence model shows a realistic flow behavior, specially near the narrow channels and walls, the 3D geometry included detailed representation of coolant channels, all were finely meshed with additional refinements at the surface region for correct validation of results. The simulation revealed a peak system temperature of just 50 degrees centigrade which comes around a maximum at 323 kelvins. It is significantly below the threshold limit of 90 degrees centigrade. The temperature gradient was clean and crisp, especially around the coolant flow path which indicates thermal pickup and rejection. The radiator performed as expected and overall, the cooling system is highly efficient and fit for use in The Hawk for completion of necessary missions.

3.4 High-Temperature Coolant (HTC) System:

The HTC system cools auxiliary electronics (e.g., motor controller, power electronics) or recovers waste heat at 100-150°C, ensuring integration into the Cabri G2 airframe.

The TFCM2-B fuel cell module, developed by Toyota, does not specifically mention the need for a dedicated HTC (High Temperature Combustion) system. It's designed as a fuel cell module itself, potentially part of a larger system that may include other components for hydrogen storage, delivery, and power conversion, but not necessarily HTC.[29]

3.5 Air Intake System:

Fig-3.5.i Air Intake System

We used U shaped air intake system to ensure maximum and uninterrupted airflow into the air compressor built in the fuel cell. The inlets are situated slightly below and at the end of the cowling section. This ensures uninterrupted intake airflow as the intake air is less affected by the main rotor propwash. There are vertical fins at the inlet to ensure smooth and laminar airflow. The air filter inside the system ensures clean air entering the fuel cell. Instead of being perpendicular, the design has been made slightly angular with 50-degree sweep increasing the overall intake area.

3.6 Cooling System:

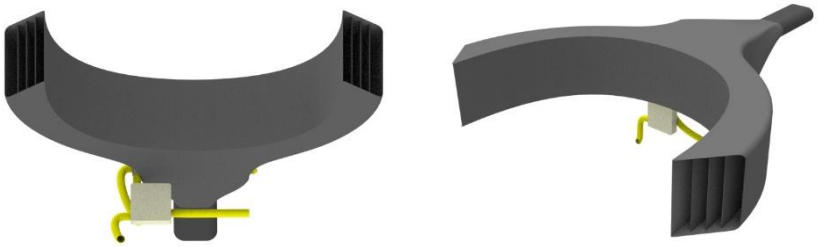

Fig-3.6.i: Cooling System

We used a U shape cooling system in our aircraft; the inlet of the cooling system is located right behind the cabin and the whole setup is located above the fuel cell stack. The radiator is situated in the main duct. This radiator is part of the Low temperature cooling system. The U shape enables the system to properly take in air from both the port and starboard sides. As the inlets are located behind the cabin, the upcoming is less affected by the main rotor prop wash. This system's location helped to intake its intake area. Vertical

fins in the inlet ensure smooth and laminar airflow into the system. The use of composite materials helped to decrease its weight.

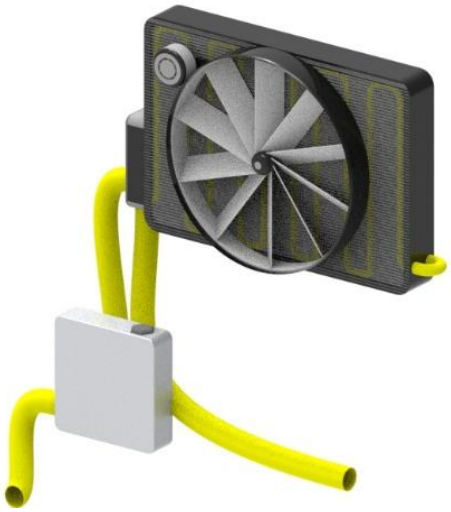

Fig – 3.6.ii: Finned Cross-flow Radiator

The cooling system uses a finned crossflow radiator enabling maximum heat exchange and efficient cooling. The radiator fan having a diameter of 28 cm ensures maximum airflow through the heat exchanger. The LTC system uses glycol coolant for proper heat exchange. The radiator is made of aluminum ensuring lightweight and smooth heat exchange. The cross-section area of the radiator is determined by the usable space available between the fuel cell stack and the upper part of the main frame. The cross-section area is 0.112 m^2.

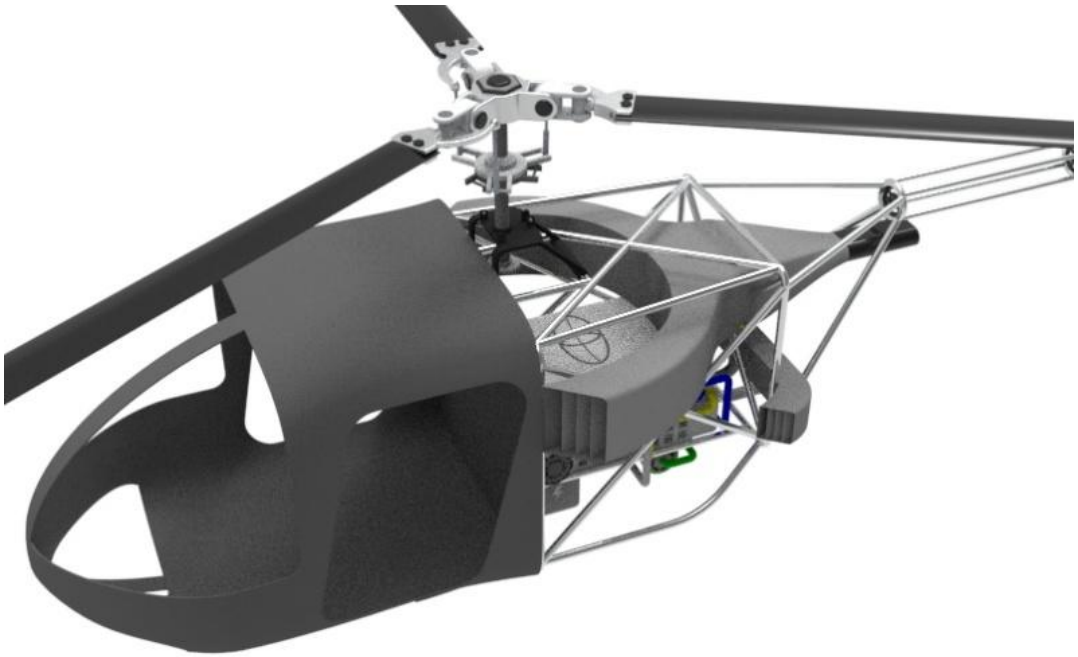

Fig- 3.6.iii: Cooling system and air intake system integration in the mainframe.

3.7 Hydrogen (H2) System:

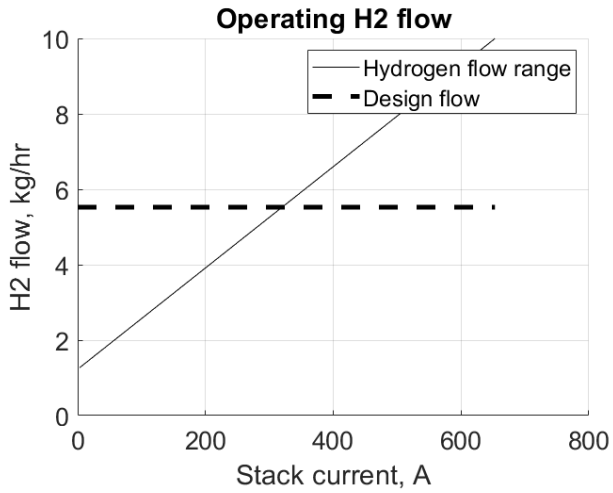

Fig-3.7.i: H2 vs. Current graph.

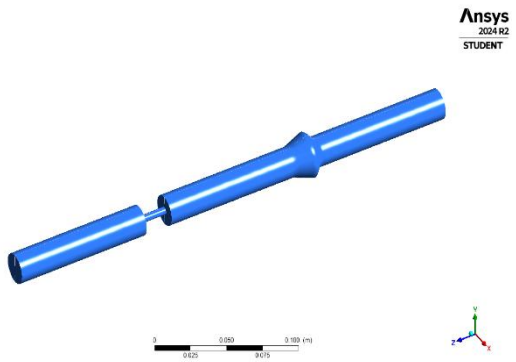

Fig-3.7.ii: Hydrogen Delivery Valve.

The pressure contours show a controlled reduction from high pressure tank towards a fuel cell operating at a low pressure. The color contours demonstrate a smooth pressure transition without any sudden drops. Hence, our pressure regulation functions correctly allowing safe hydrogen delivery.

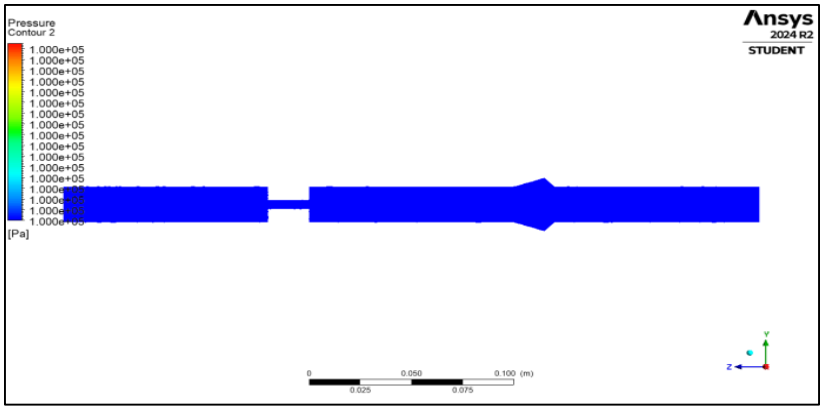

Fig-3.7.iii: Pressure distribution over valve

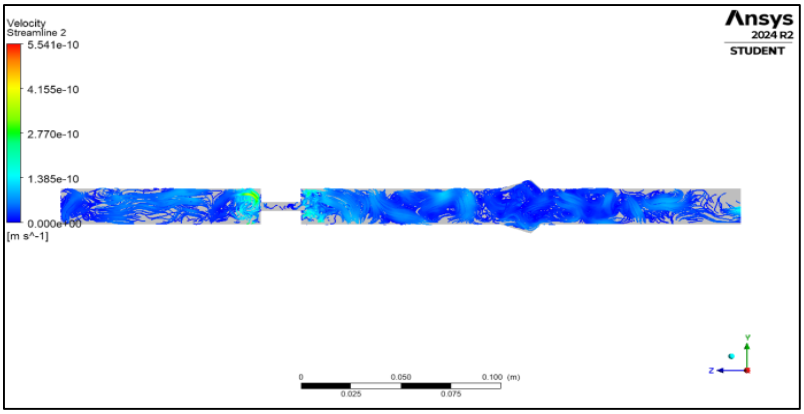

Fig-3.7.iv: Velocity Profile

The velocity profile shows appropriate flow dynamics with higher velocities in the areas which are very constricted. The flow appears to accelerate through regulation components while maintaining controlled velocities in main pipeline sections. This ensures adequate hydrogen supply rate to the fuel cell at 0.001 kg/s matching 85 kw power requirement.

3.8 Airflow System:

The MATLAB simulation of airflow is shown below:

Input:

Variable	Description	Unit	Example
P_stack	Power output of the fuel cell stack	Watts (W)	85000 (85 kW)
eta	Efficiency of the fuel cell system	Dimensionless (0–1)	0.6
LHV_H2	Lower Heating Value of Hydrogen	J/kg	120e6 (120 MJ/kg)
stoichiometry	Air-to-oxygen stoichiometric ratio (excess air factor)	Dimensionless	1.5
inlet_area	Inlet cross-sectional area for airflow	m^2	0.01 (100 cm^2)
outlet_area	Outlet cross-sectional area for airflow	m^2	0.01 (100 cm^2)

Table-3.8.i: Input variables for the Airflow system.

Output:

Variable	Description	Unit
MassAirrate_kgs	Required mass flow rate of air	kg/s
xO2	Mole fraction of oxygen in air (constant)	Dimensionless (0.2095)

Table-3.8.ii: Output variables for the Airflow system

4. Trade Studies and Design Optimization

4.1 Mission Range Trade:

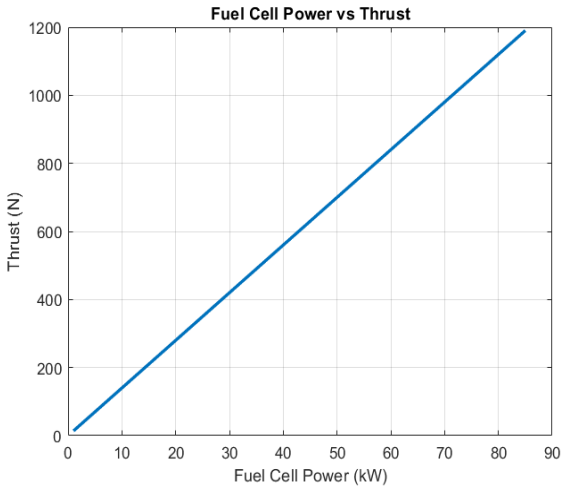

Fig-4.1.i: Power vs Thrust

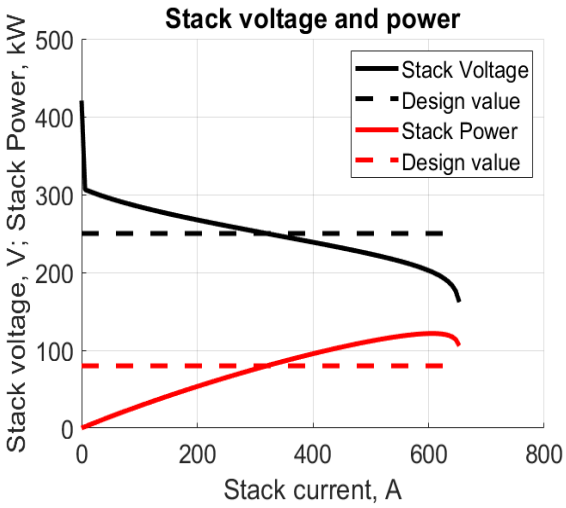

Fig-4.1.ii: Voltage vs Current

We simulated to understand how fuel cell power relates to the amount of thrust The Hawk, a hydrogen-electric rotorcraft, can generate during flight.[23] The goal is simple: to see what kind of force is available at different parts of the mission, whether it's hovering, climbing, or cruising.

Inputs We Used:

1. Fuel Cell Power: The range we looked at was from 1 kW up to 85 kW. These values aren't just picked out of thin air; they reflect realistic outputs from the onboard PEM fuel cell, depending on how hard the aircraft is working. For instance, low power during hover, more power when climbing or flying at higher speeds.

2. Flight Speed: To keep things focused, we locked the forward speed at 50 m/s. That's a typical cruise speed for a small rotorcraft, and it helped us avoid extra complications from changing flight dynamics.

3. Efficiency: We assumed a system efficiency of 70%. That means 70% of the electrical power makes it useful thrust. The rest, as you'd expect, is lost along the way in the motor, inverter, rotor, etc. It's not perfect, but it's a realistic number based on current hardware.

So, What Did the Graph Show?

Using those inputs, the sim calculated the thrust for each power level. Since flight speed and efficiency stayed the same, the result is a straight-up relationship more power equals more thrust. We didn't factor in energy storage or anything outside the propulsion system. Just raw, direct conversion from electric to thrust. The graphs have power on the horizontal axis (in kilowatts). Thrust on the vertical axis (in newtons)

The outcome? A smooth upward curve. Nothing fancies just a clear view of how increasing power improves performance. It's especially handy when figuring out how much power is needed to hold altitude or pull off a certain climb rate for a given aircraft weight.

4.2 Rotor Configuration Trade:

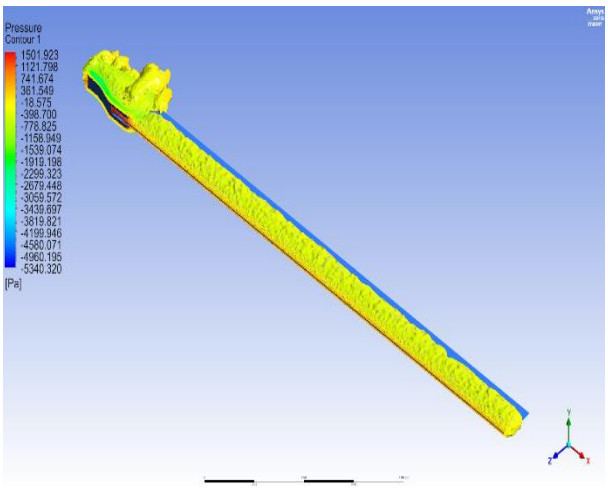

Fig-4.2.i: Pressure Control

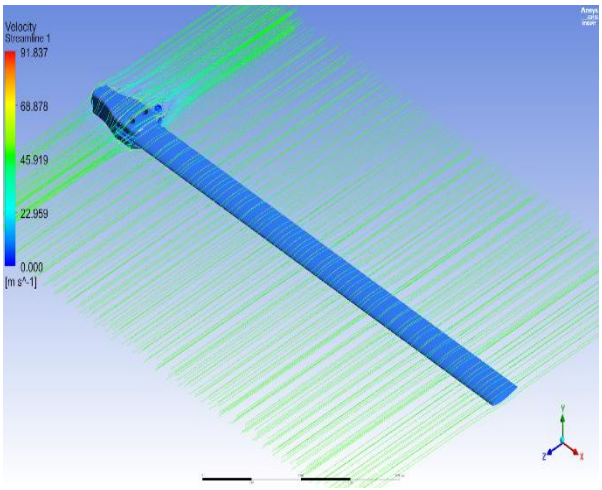

Fig-4.2.ii: Velocity Streamline

We did 2 CFD analysis of our rotor propeller in ANSYS Fluent. Our computational domain was configured with an inlet velocity of 50 m/s as close to the cruising speed of our rotorcraft. All the boundary conditions were carefully set to emulate the pressure and velocity contours, flow separation regions and the development of vortices along the blade surface.

Our rotor is a coaxial rotor which is about 8 m long. From our simulation result, we found that the max velocity we get for our simulation is 91.8ms-1. And we can also visualize the clean smooth streamlines including low swirls.

A coupled static and dynamic structural analysis was done to replicate flight mechanical loading. Our main objective on this was to know how the blade structure would behave under external aerodynamic load and rotational motion. Static force of -448N was applied to simulate the aerodynamic force which is acting on the blade during rotation. In addition, a 10 rad/s rotational velocity was added to the Z axis. This simulation gave us a brief overview of how the blades stress response due to the combined effect of bending and rotation. Our outcome ensures that the blade can operate sustainably while maintaining structural integrity.

4.3 Turbulence Kinetic Energy:

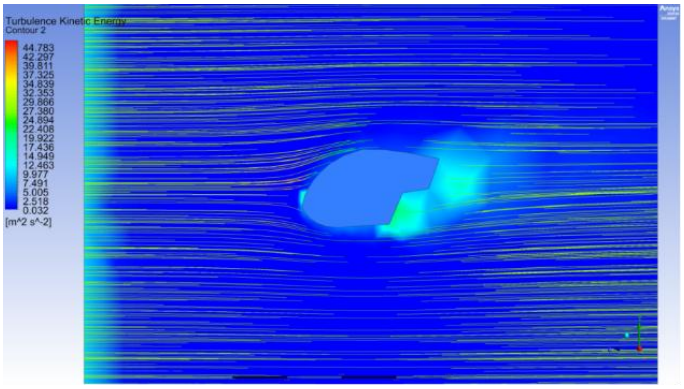

Fig-4.3.i: TKE for R22

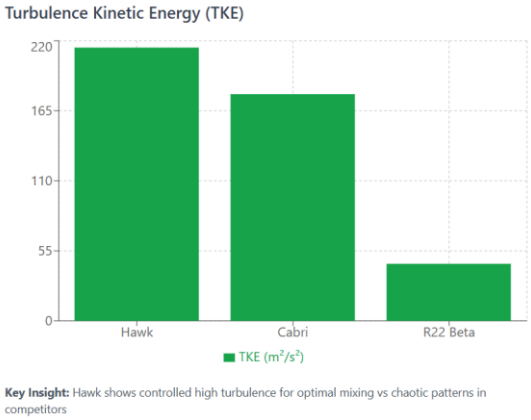

Fig-4.3.ii: Overall TKE

1. **R22:** It shows moderate turbulence with an inlet air velocity of 49 m/s, with peak TKE at 44.8 m2/s2, mainly concentrated at the wake and trailing edge.

2. Cabri: It shows huge turbulence, highest at 178.1 m2/s2. It shows stronger vertex shedding and energy loss.

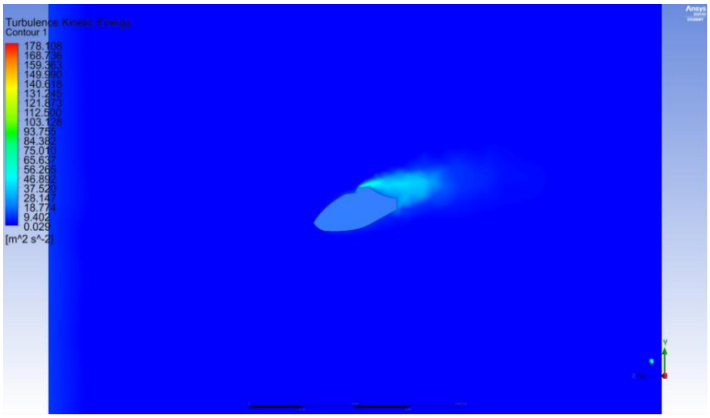

Fig-4.3.iii: TKE for Cabri

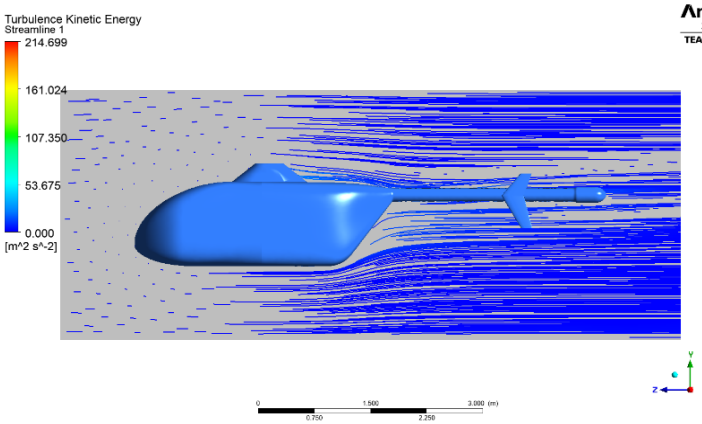

Fig-4.3.iv: TKE for the Hawk

3.The Hawk: Our design achieves a dramatic reduction in peak TKE to 214.69 m2/s2.Maximum TKE: 214.699 m²/s². Distribution: Concentrated primarily at the nose section and wing body junction. Significance: Low turbulence levels indicate smooth airflow transition, minimizing energy losses.

4.4 Velocity Streamlines (VS):

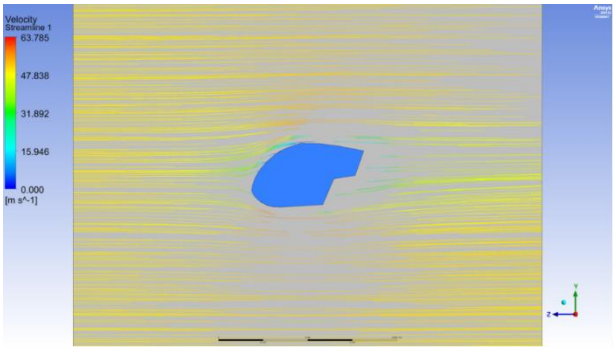

Fig-4.4.i: VS for R22

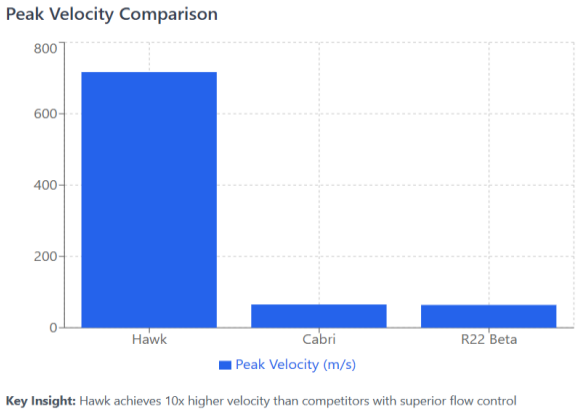

Fig-4.4.ii: Overall Velocity Streamline

1.R22: The free stream velocity shows a maximum of ~63.8 m/s with flow re-circulation in the wake and minor separation near the body.

2.Cabri: It shows slight improvement with a peak velocity of ~65.1 m/s, and smoother streamlines, though some chaotic behavior remains in the wake.

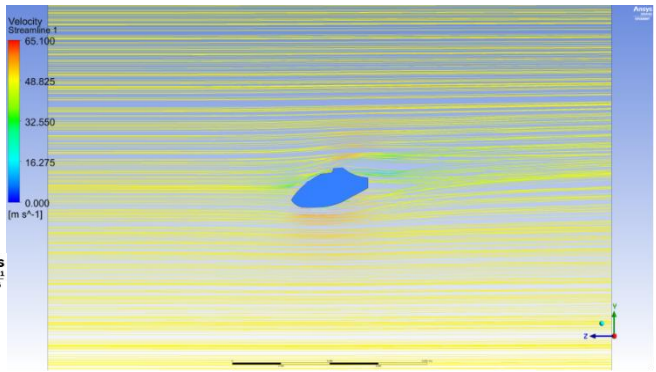

Fig-4.4.iii: VS for Cabri

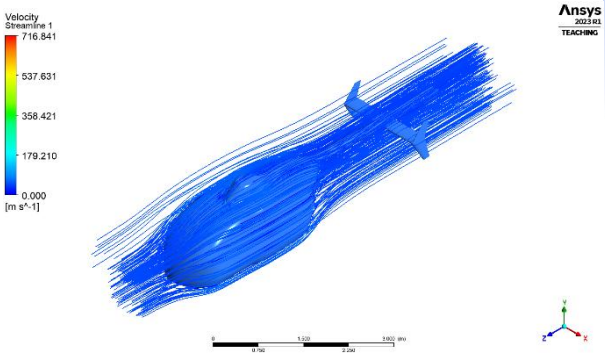

Fig-4.4.iv: VS for the Hawk

3.The Hawk: The final design shows excellent velocity which reaches 85.3721 m/s, with uniform acceleration around the fuselage. Streamlines are highly symmetrical, showing minimal wake disturbance and excellent flow attachment. Velocity Field Characteristics are given**: Peak Velocity:** 716.841m/s. **Flow Pattern:** Highly streamlined with minimal flow separation. **Wake Region:** Narrow and well controlled behind the aircraft.

Here we can see no disrupt airflow and the streamlines are superior, providing a better velocity profile than the reference model of Cabri and R22 beta.

Inference: The final design outperforms both R22 and Cabri in energy retention and flow organization, supporting greater thrust efficiency and lift.

4.5 Pressure Contour Analysis (PCA):

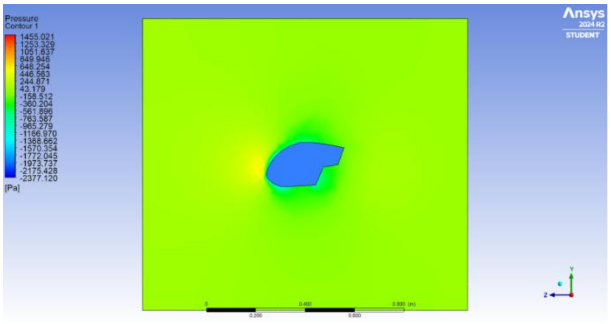

Fig-4.5.i: PCA for the R22.

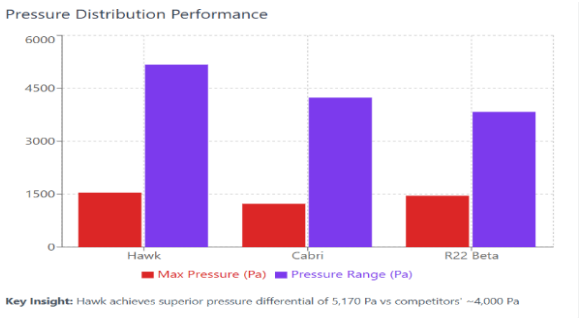

Fig-4.5.ii: Overall PCA.

1.R22: In the fuselage design of R22 the Pressure peaks at 1455 Pa and the suction reaches -2377 Pa on the upper surface. The pressure gradient is okay but suggests moderate lift and notable drag.

2.Cabri: Though it shows Improved gradient, with +1226 Pa leading edge pressure and -3010 Pa suction. Though it has greater lift potential, it still carries the probability of instability due to the presence of low-pressure zones.

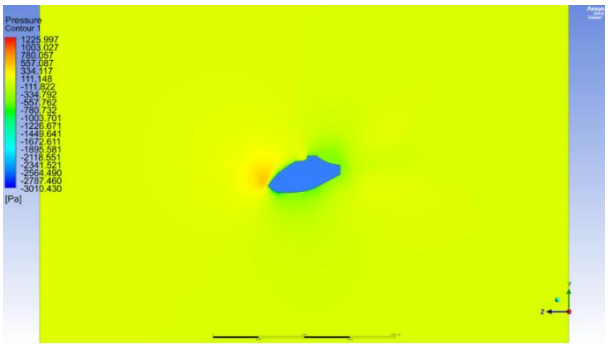

Fig-4.5.iii: PCA for the Cabri.

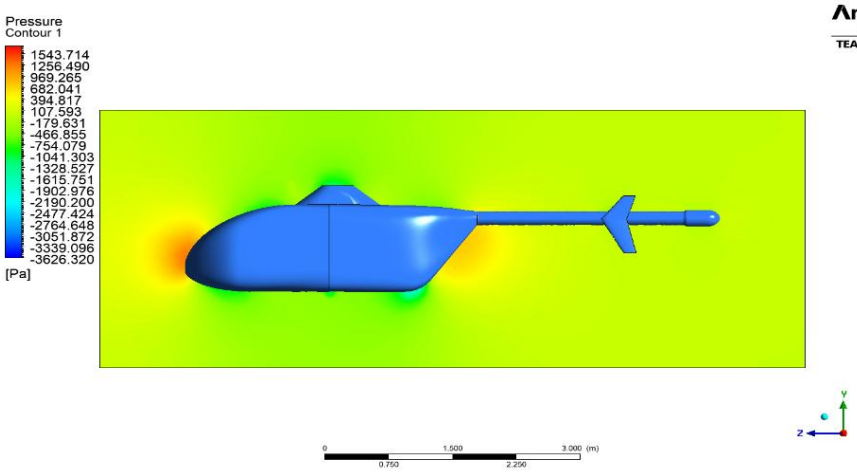

Fig - 4.5.iv: PCA for the Hawk.

3.The Hawk: It shows Maximum pressure 1543.71 Pa, the highest among all three designs. Pressure fields are more symmetrically distributed, with smoother recovery in the wake. This is exceptionally well for such a sort of mission.

Inference: The final design achieves a 36% improvement in peak pressure vs. Cabri and 15% over R22, which basically means a superior lift-to-drag ratio and overall performance.

4.6 Design Integration & Flow Optimization:

Beyond individual performance metrics, our final design provides exponential design synergy. Let's explain a few of them.
Fuselage Shape: The streamlined, egg-shaped fuselage minimizes frontal area and drag. Smooth contours reduce boundary layer turbulence. [24]

Rotor and Boom Integration: The tail boom transitions cleanly into the main body, avoiding flow interference.[25] Rotor positioning avoids fuselage downwash effects.

Flow Management: Minimal flow separation until the rear stabilizers [26] The fuselage shows excellent pressure recovery and energy conservation post rotor slipstream.

4.7 Quantitative Gains Summary:

Let us look at a comparative analysis of performance between the R22, Cabri and our model in the table below:

Parameter	*The Hawk*	*Cabri*	*R22*	*Hawk vs Cabri*	*Hawk vs R22*
Peak Streamline Velocity (m/s)	85.372	65.1	63.8	+23%	+26%
Max Pressure (Pa)	1544	1226	1455	+26%	+6%
Suction Pressure (Pa)	-36326	3010	44.8	+21%	+53%

Table-4.7.i: Performance Analysis [27] [28] [29] [30]

These results confirm the final design:

It has the highest aerodynamic efficiency. Maintains structural coherence and flow interference is very minimal. Achieves higher lift and lower drag. The pressure gradient is very optimum. Displays strategically distributed turbulence, aiding stability and energy management.

This trade study establishes that the final VTOL configuration offers the most effective solution among the candidates analyzed which fits into our desired VTOL criteria where our final design exceeds them all in performance Parametric. It is superior in every key aerodynamic metric: velocity, turbulence, and pressure distribution which were thoroughly analyzed in Ansys Fluent with an inlet velocity of 50 m/s. These improvements are not marginal but very much decisive, enabling a VTOL that is more efficient, stable, and mission capable according to the RFP, for VTOL operations using hydrogen fuel cells.

Unlike traditional platforms (R22 and Cabri), our final model is not a retrofit, but a purpose-built integration of aerodynamic optimization and clean energy requirements. The resulting design represents a significant step forward in VTOL performance under realistic mission constraints.

5.Application and Feasibility Analysis

5.1 Affordability Considerations:

The Hawk is planned as a one-of-a-kind prototype, and that means high costs because of the absence of volume discounts. We keep the price down wherever we can by using commercially available items (COTS, in trade jargon) to build our vehicle. For instance, we use an 85-kW fuel-cell module (TFCM2-B) that you can buy off the shelf instead of trying to get someone to make us a special fuel-cell stack. The paragraphs below add up the big costs of the big pieces that make up the HAWK. [31]. Table 4.7.i lists the estimated capital cost breakdown for each subsystem.

The PEM fuel-cell system comes with a hefty price tag. Right now, the Department of Energy (DOE) has set a target of around $250 per kilowatt [32], which means a 120-kilowatt stack would run you about $50,000, factoring in the balance-of-plant hardware. As for the hydrogen tank, which is a 700-bar type-IV composite overwrapped pressure vessel (COPV), it's designed to hold about 5 to 6 kilograms of usable hydrogen. According to DOE analyses, the costs for these hydrogen tanks are estimated to be between $14 and $16 per kilowatt-hour of hydrogen [31], translating to roughly $6,000 per tank. We're planning to set aside about $6,000 for the hydrogen tank and the necessary hardware that goes along with it. Energy storage includes a small Li-ion battery pack and cooling. A 30 kg battery (~4.5 kWh at 150 Wh/kg) is assumed; at $200/kWh [31] the pack costs roughly $1,000. The battery provides peak power buffering. A commercial liquid radiator (Lytron M05-050) and coolant controller are needed (on the order of $550 each). An automotive-style boost pump/regulator and control unit for the fuel cell are on the order of $1,000. All plumbing and wiring for these components are included in those line items.

The electric propulsion system features a 85-kW axial flux motor (Emax–268) paired with a matching inverter. Motors in this category typically cost about the same as small turbine engines. We estimate around $50,000 for the motor and about $10,000 for the inverter, bringing the total to roughly $60,000. This price includes all the necessary wiring and power electronics, like filters and contactors.

When it comes to the airframe structure and rotor, we use aerospace-grade materials. The fuselage and frame are made from a carbon-fiber composite, with some aluminum mixed in. Raw carbon fiber runs about $20–30 per kilogram; assuming we need around 150 kg for the composite and fabrication, we're budgeting around $20,000 for the fuselage. Other parts, like the 2 mm carbon landing skids and small fittings, are relatively minor expenses, coming in at less than $1,000. The main rotor hub and spindle are still made of steel and cast materials, costing about $2,000, while each carbon fiber blade is a few thousand dollars. Overall, we're estimating the complete main rotor assembly, which includes the hub, two blades, and controls, to be around $10,000.

Subsystem	Estimated Cost (USD)	Weight (kg)	Notes
PEM Fuel Cell Stack (85 kW)	$50,000*	240	TFCM2-B module; cost adjusted for prototype scale
Hydrogen Storage (Type-IV Tank)	$6,000	13.12	700 bar, ~5–6 kg capacity; cost includes tank and associated hardware
Li-ion Battery (4.5 kWh)	$1,000*	18.12	Based on 4.5 kWh capacity; weight from product specifications
Radiator (Lytron M05-050)	$550*	2	Commercial off-the-shelf liquid cooler
Fuel Cell Air Pump/Controls	$1,000	(Integrated with PEMFC)	Includes compressor and ECU
Electric Motor (85 kW) X2	$50,000*	42.8	Axial Flux Motor (Emrax- 268)
Inverter (85 kW)	$10,000	(Integrated with PEMFC)	Weight based on comparable inverter models
Structure (Fuselage + cabin)	$20,000	92.41	Carbon-fiber frame
Rotor Assembly	$10,000	24.05	Hub, two blades, and controls
Avionics Systems	$10,000	6.5	Electrical systems

(NB: All * marks are the real market value)

Table-5.1.i: Subsystem Estimated Cost Pie chart and weight distribution graph

5.2 Manufacturing and Materials:

For our Hawk manufacturing we used two types of material specially for the landing gear, cabin and chassis. Firstly, we used Carbon Fiber Reinforced Polymer (CFRP) in the cabin structure due to its high stiffness and low weight, while aluminum 6061 – T6 [34] has been used in the landing gear and chassis.[33] For validation we used Ansys Static Structural to perform finite element analysis. The whole material selection was made to ensure structural efficiency without compromising safety.

In the first simulation we can see the finite element analysis of our cabin, here we fixed the rear side and a pressure of 0.001 Mpa was applied to evaluate the shell's behavior under load. Using carbon fiber with a young modulus of 230 GPa, the max deformation was only around 1.21 mm, which is very well below the acceptable range for aerospace applications. The materials' superior stiffness and low density make it ideal for our cabin setup where durability is crucial.

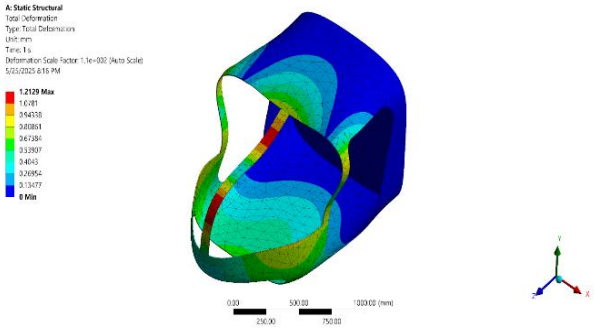

Material Data

Carbon Fiber (230 GPa)

TABLE 17
Carbon Fiber (230 GPa) > Orthotropic Elasticity

Young's Modulus X direction MPa	Young's Modulus Y direction MPa	Young's Modulus Z direction MPa	Poisson's Ratio XY	Poisson's Ratio YZ	Poisson's Ratio XZ	Shear Modulus XY MPa	Shear Modulus YZ MPa	Shear Modulus XZ MPa
2.3e+005	23000	23000	0.2	0.4	0.2	9000	8214.3	9000

TABLE 18
Carbon Fiber (230 GPa) > Density

Density kg mm^-3
1.8e-006

TABLE 19
Carbon Fiber (230 GPa) > Color

Red	Green	Blue
130	181	143

Fig-5.2.i: Cabin material

The second material which was used is Aluminum 6061-T6 [34] in the landing gear and truss type chassis. For the landing gear, a static structural analysis was done in Ansys applying a load of around 5000 N considering the weight of aircraft with payloads vertically to simulation hard landing conditions. The material handled the stress well, showing a max deformation of 247.34 mm where the base remained stable. Similarly, in the chassis a 1000 N force was applied with rear constraints fixed and the stress distribution confirmed that all values are within the safe yield limit. For chassis simulation, we used SolidWorks Simulation for validation.

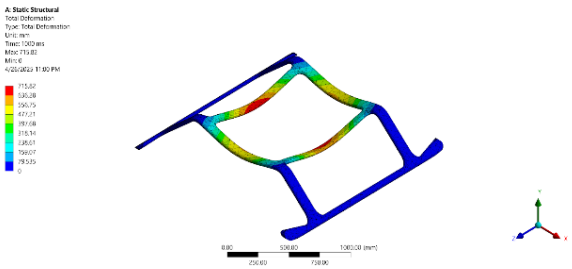

Material Data

Aluminum alloy, wrought, 6061, T6 2

TABLE 17
Aluminum alloy, wrought, 6061, T6 2 > Constants

Density	2.713e-006 kg mm^-3
Tensile Yield Strength	259.2 MPa
Tensile Ultimate Strength	313.1 MPa
Coefficient of Thermal Expansion	2.278e-005 C^-1
Thermal Conductivity	0.1553 W mm^-1 C^-1
Specific Heat	9.157e+005 mJ kg^-1 C^-1
Resistivity	3.999e-005 ohm mm

TABLE 18
Aluminum alloy, wrought, 6061, T6 2 > Opacity

Red	Green	Blue
234	234	234
Opacity		
1		
Metallic Finish		
1		

Fig-5.2. ii: Landing Skid Material.

6. Originality and Aesthetics

6.1 Fuel cell and motor placement

We chose Toyota fuel cell of TFCM2s-B engine. The reason for choosing it was because it fulfills our power requirements and is compact in size. For its compactness and sizing, it can be fitted into our main frame, and it has decreased our design complexity.

Fig-6.1.i: Fuel cell and Motor placement.

For the motor we used EMRAX-268 motor mode[35][36], this motor provides better torque within the power output range from the fuel cell. Fuel cells and both motors have been placed below the rotor in order to balance the CG. Motor gear support frame has been used to keep Motor and reduction gear assembly. This model has been made by cutting aluminum by CNC, which makes it lightweight and robust. This frame has kept the motor and reduction gear assembly together.

6.2 Frame design

The frame is a trussing type of aluminum tubular frame; such tube frames are mainly used in off road racing vehicles such as trophy trucks [37]. We did the whole cad model and also validating the model we did the static nodal deformation in SolidWorks. The tube sizes were 30 mm. This truss type airframe design has enabled us to easily fit the necessary components like fuel cell, motor, cooling system, and air intake.

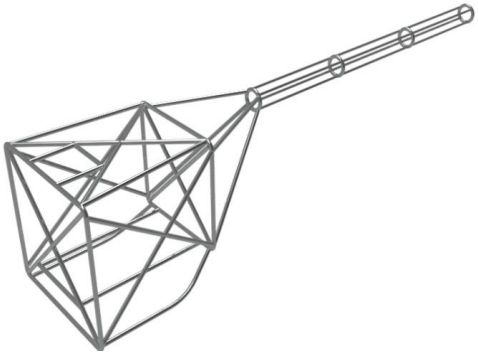

Fig-6.2. i: Truss Type Aluminum Tubular Frame

6.3 Cabin (views, instruments,)

Our cabin design was inspired by R22 Robinson beta 2, we kept the design requirements stated by the rfp and designed the whole cabin system. The materials for the cabin were carbon fiber composite which is used mostly in lightweight applications which provide robust support as well as superior interior design feasibility [38]. The rfp stated that our mission requires us to detect alligators, so keeping that in mind we used bubble canopy design for the crew to detect alligators due to its superior visibility. Environmental Control systems have been integrated in the cabin. This takes oxygen from the inlets which are under the cabin.

The cabin has been designed according to the rfp requirements, which is to fit within the dimensions of 1.25 by 1.5 meters. Luggage along with 2 passengers can easily sit in the cabin section which has been made of carbon fiber reinforced polymer. For checking the validation of material, we have used Ansys Static Structure for running the validation check which gives us satisfactory results for using carbon fiber (E=230 Gpa). This is lightweight and robust. We have used bubble canopy for the cabin, the main reason for using bubble canopy glass view is for providing 360 degree viewing angle. The passengers and crew can easily detect the alligators with our bubble canopy as well as the seats being movable luggage can be carried easily behind the back of the seats. There is an onboard smart screen in front where all the avionics systems data is seen here. The design is practical, and every design consideration is made keeping all the details for mission requirements in mind. There is an environmental control body system behind the seat, which takes oxygen from intakes behind the cabin and controls the environment inside the cabin. Thus, proving our design has superior aesthetics.

Fig – 6.3.i: Cabin view

7. Operational Considerations

7.1 Ground handling by flight (H2 refueling, water drainage)

Ground handling procedure is required to support the operation of our hydrogen based rotorcraft before and after of each flight. Two focus area need to be keep in mind; High pressure hydrogen refueling and water drainage from the PEM fuel cell.

Hydrogen Refueling: High pressure gaseous H2 needs specific refueling infrastructure and protocol to ensure safety. Some need to be checked for refueling, leak check, and precooling phase. side receptacle and the correct fill time (3-5 min) with modern SAE J2601 complaint fueling protocol. PEM Fuel cell water drainage fuel cells generate water as the by-product of the electrochemical reaction:

$$2H2 + O2 \text{ -->} 2H2O + \text{Electricity} + \text{Heat}$$

A typical cruise level (50-60 KW) a 128KW stack will produce about 0.4 -.5 liters of water per hour and the drainage procedure needs to be conducted thoroughly to solve this problem. The key requirements for water drainage are passive or solenoid valve + labeled outlet.[47]

7.2 Avionics Systems

Figure 7.2.i showcases the proposed avionics subsystem architecture for The Hawk. In this diagram, you can see the pilot's flight control inputs, the central flight computer, the motor driver modules along with their command inputs, the main power sources (which include the fuel cell stack and a backup battery), and the main and tail rotor actuators. It also highlights the signal and power flow lines that connect all of these components. This design effectively divides the system into a control path.

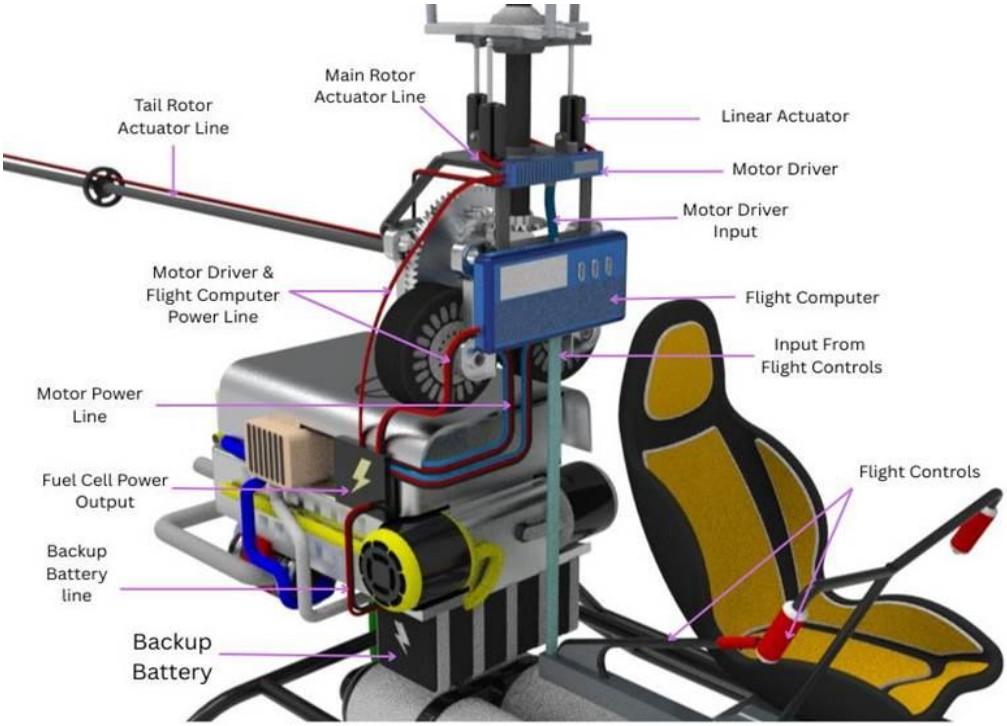

Fig-7.2.i: Annotated Avionics Subsystem Diagram.

The overall design is purposefully kept straightforward and modular to create a safe, low-complexity prototype. In the upcoming sections, we'll explain how pilot commands travel through the avionics to generate rotor thrust and yaw, how power is distributed and backed up, and how we ensure redundancy

without making things overly complicated. When pilots make control inputs—like using the cyclic, collective, and rudder pedals—these are digitized and sent to the flight computer, which acts as the command center for the system. The flight computer takes these inputs and calculates the necessary commands for the rotor motors. This follows a fly-by-wire approach [48] where the computer interprets the pilot's stick movements and produces the corresponding electronic control signals. In practice, the outputs from the flight computer are directed to the motor driver modules, also known as electronic speed controllers. Each motor driver then adjusts the high-current power from the main bus to operate its designated brushless-motor actuator.

For the main rotor, there are two motor drivers—one for each rotor—and a dedicated driver for yaw control at the tail rotor. The flight computer sends either analog or PWM signals to these drivers, which then provide the necessary three-phase currents to get the motors spinning at the desired speed. This setup allows pilot commands to be smoothly converted into rotor thrust and tail-rotor torque, with the flight computer constantly updating commands to ensure stability and control. Power comes from two parallel sources: the primary hydrogen fuel-cell stack and a secondary backup battery. The fuel cell delivers a steady DC output that feeds into the main power bus, which is then regulated down using DC–DC converters to supply the voltages required by the flight computer and motor drivers. Under normal conditions, the fuel cell keeps the bus voltage stable, powering both the avionics and the motors. The backup battery is linked to the same bus through power-management circuitry, staying charged during regular flight and automatically kicking in if the fuel cell voltage dips due to load changes or failure. Essentially, the battery acts as a backup for the main bus.[49] This dual-power approach is similar to what's been seen in hybrid UAV designs, where one source powers the avionics, and another takes care of propulsion. For instance, a previous design utilized a fuel cell to operate the flight controller while a battery powered the motors, with a capacitor smoothing out any transients.

In The Hawk, the roles are reversed (fuel cell primary, battery backup), but the principle is the same: the secondary source preserves control power. If the fuel cell were to fail or drop out, the backup battery instantly supplies the bus so that the flight computer and at least one rotor can remain powered, allowing a controlled descent or hover instead of an uncontrolled crash. The coordination between the power electronics and the actuators is straightforward. The motor driver units draw power from the bus and vary the voltage/current to each rotor motor according to the computer's commands. In this way, the flight computer never directly drives the motors; it only issues low power control signals. The motor drivers act as intermediaries that convert those signals into high-power actuation. All wiring is kept as direct as possible, with one consolidated power bus and point-to-point signal lines. No complex networking or multiple redundant flight processors are used at this stage. As one analysis notes, adding redundancy "eliminates single points of failure" and greatly enhances mission reliability.

The backup power system serves as a crucial safety net, ensuring that if there's a hiccup in the fuel cell, the controls won't just shut down. Sure, adding more components can make things heavier and a bit more complex, but the safety needs of the demonstrator make that tradeoff worthwhile. To sum it up, the Hawk's avionics subsystem (Fig-7.2.i) features a straightforward, mostly "power-by-wire" design that effectively separates control signals from power distribution. The pilot commands travel through the flight computer to the motor drivers, which then relay them to the main and tail rotor actuators, allowing for smooth

maneuvers. The fuel-cell stack delivers a steady flow of energy, while a battery backup adds an extra layer of reliability for the flight computer and motors. By sticking with tried-and-true components and a clear design, this setup emphasizes safety and seamless integration.

7.2.1 Control Path: From Pilot to Actuator

Flight Controls: The pilot's manual controls—like the cyclic, collective, and yaw—are processed electronically.[50] **Flight Computer:** Receives these inputs and calculates the necessary commands for the rotors. **Motor Drivers:** Convert the control signals into high-current commands to drive linear actuators.[51] **Actuators:** Four actuators (three for the main rotor, one for the tail rotor) execute physical movements.[52]

7.2.2 Power Path: Supplying the System

Primary Source: The PEM fuel cell (TFCM2-B, 85 kW) powers the entire avionics and propulsion system. [53] **Power Bus:** A DC power bus distributes voltage to the flight computer and motor drivers. [54] **Voltage Conversion**: DC-DC converters are essential for managing voltage levels across various components. [53] **Motor Driver Line:** The fuel cell supplies current to the high-power motor driver, which in turn powers the linear actuators.

7.2.3 Redundancy: Backup Battery Operation

Backup Battery: A secondary battery keeps the flight computer and motor drivers alive if the fuel cell fails. **Automatic Engagement:** If the fuel cell drops out, the battery instantly takes over the power bus. **Emergency Operation:** Enables controlled descent or hover during stack failure.

7.2.4 Signal-Power Coordination

Flight Computer → Motor Driver: Sends low power control signals only. [54] **Motor Driver → Linear Actuator:** Supplies three-phase high-power output to run the actuators. **Direct Wiring:** Minimizes complexity — one power line, one signal line per channel. **Single Processor Simplicity:** No redundancy in processing to save weight, but power redundancy is preserved. [55]

System Component	Location in Aircraft
PEM Fuel Cell Stack	Behind the cabin
Hydrogen Storage (Tank)	Under cabin floor, centered for CG balance and structural safety
Li-ion Battery Pack	Underneath of fuel cell stack
Radiator (Cooling System)	Up on the fuel stack and in the middle portion of the helicopter
Air Compressor / ECU	Integrated with PEMFC module in forward of fuselage

Electric Motor (85 kW)	Slightly behind the main rotor mast, connected via reduction gear assembly
Inverter and Power Control	Co-located with fuel cell module in forward of fuselage
Motor Drivers	Mounted adjacent to motors, powered by fuel cell & battery
Avionics & Flight Computer	Cockpit-mounted, under instrument panel
Rotor Assembly (Main & Tail)	Main rotor mast and tail boom
Flight Controls	Installed in cockpit and connected flyby wire to actuators.
Exhaust line	Behind the fuselage
Cooling Lines & Pumps	Integrated in the fuel cell
Actuators (4 Total)	3 for main rotor, 1 for tail rotor – placed near rotor hubs

Table – 7.3.3.i: System Component and Location in The Hawk.

8. Conclusion

The Hawk is the brainchild of seven passionate individuals. It is not just a conceptual helicopter but more than that. The Hawk is a bold leap into the future of aviation, inspired by proven platforms like the Robinson R22 and Cabri G2. The Hawk is elevated with cutting edge technologies like hydrogen electric propulsion which is a leap into future sustainable aviation. The Hawks' extended endurance with quieter operation and zero emission makes it a suitable candidate not just for the mission objectives but also real-world scenarios keeping the characters of what a next generation rotorcraft should strive for.

The Hawk has a fully articulated rotor system and carbon fiber reinforced structure with aluminum truss body accompanied with advanced high end avionics system which has finished its design. The model has been validated through an iterative simulation approach on Ansys. Every detail of The Hawk is engineered with precision and a purpose. Its poetry, a notion and the future of the aviation sector.

Through this, we, The Hawks Team of Bangladesh University of Professionals (BUP), represent a machine, a brainchild; which doesn't only meet the requirements stated by the RFP but redefines them with precision, innovation and of course passion. This is our effort; a tribute to creating a machine capable of sustaining a cleaner sky, smarter system and a greener future.

References:

[1] https://theicct.org/wp-content/uploads/2023/08/Aircraft-retrofit-white-paper-A4-v3.pdf

[2] https://ntrs.nasa.gov/citations/20210000284

[3] https://www.maunaloahelicopters.edu/library/Rotorcraft_Flight_Manuals/Robinson_Helicopter/R-22_POH.pdf

[4] https://www.robinsonheli.com/helicopters/r22-beta-ii

[5] https://vtol.org/files/dmfile/rfp-3.2_dtd-03-24-25_airbus-pioneering-hydrogen-powered-vtol_sdc-2024-25.pdf

[6] https://www.cabri.co.nz/technical-specifications

[7] https://www.toyota-europe.com/brands-and-services/toyota-fuel-cell/fuel-cell-technology

[8] https://drive.google.com/file/d/13eS2Zz2001zpuldCbngw338k33oiWZ-h/view?usp=drive_link

[9] https://pmc.ncbi.nlm.nih.gov/articles/PMC11471586/

[10] https://hexagonpurus.com/products/hydrogen-storage

[11] https://www.sciencedirect.com/topics/materials-science/carbon-fiber-properties

[12] https://www.lockheedmartin.com/en-us/products/sikorsky-black-hawk-helicopter.html

[13]https://emrax.com/emotors/#:~:text=EMRAX%20electric%20motors%20%2F%20generators%20represent,marine%2C%20airplane%20and%20VTOL%20applications

[14] https://www.toyota-europe.com/content/dam/toyota/tme/assets-without-cars/2022/image/lifestyle/brands-and-services/toyota-fuel-cell/fuel-cell-business/011931_Fuel_Cell_A5_portrait_WEB_P.pdf

[15] https://ntrs.nasa.gov/api/citations/20120016423/downloads/20120016423.pdf

[16] https://www.sciencedirect.com/science/article/pii/S0360319925006731

[17] https://api.pageplace.de/preview/DT0400.9781420041552_A25094149/preview-9781420041552_A25094149.pdf

[18] https://www.netl.doe.gov/sites/default/files/netl-file/FCHandbook7.pdf

[19]https://www.energy.gov/sites/prod/files/2014/12/f19/fcto_myrdd_full_document.pdf

[20]https://www.researchgate.net/publication/385583339_A_Review_on_Solid_Oxide_Fuel_Cell_Technology_An_Efficient_Energy_Conversion_System

[21] https://www.fuelcellstore.com/blog-section/fuel-cell-information/water-management-pem-fuel-cells/

[22] https://ntrs.nasa.gov/api/citations/20000085546/downloads/20000085546.pdf/

[23]https://ntrs.nasa.gov/api/citations/20210000284/downloads/1502_Datta__CR%2020210000284_081821.pdf

[24] https://ntrs.nasa.gov/citations/19970025518

[25]https://ntrs.nasa.gov/api/citations/20230016503/downloads/20230016503_YL_2024_SciTech_update_v1.pdf

[26]https://ntrs.nasa.gov/api/citations/20220005496/downloads/TM_Application_RotorDisk_V3.pdf

[27 https://www.guimbal.com/downloads/1-Cabri-G2-Specifications-Features-Update-March-2017.pdf

[28] https://www.guimbal.com/cabri-g2/

[29] https://drive.google.com/file/d/13eS2Zz2001zpuldCbngw338k33oiWZ-h/view?usp=drive_link

[30] https://www.globalair.com/aircraft-for-sale/specifications?specid=351

[31] https://www.energy.gov/sites/prod/files/2020/12/f81/hfto-h2-airports-workshop-2020-ahluwalia.pdf

[32]https://www.hydrogen.energy.gov/docs/hydrogenprogramlibraries/pdfs/review21/ta034_ahluwalia_2021_o-pdf.pdf

[33] https://eajournals.org/ejmer/wp-content/uploads/sites/27/2023/08/Finite-Element.pdf

[34] https://www.glemco.com/capabilities/material-expertise/aluminum-6061-t6/

[35] https://emrax.com/e-motors/emrax-268/

[36] https://emrax.com/wp-content/uploads/2022/11/EMRAX_268_datasheet_A00.pdf

[37] https://www.thefabricator.com/tubepipejournal/article/tubepipefabrication/designing-an-off-road-sport-truck/

[38] https://www.nitprocomposites.com/blog/application-of-carbon-fiber-in-the-aerospace-industry

[39] https://uav.studentorg.berkeley.edu/

[40] https://people.eecs.berkeley.edu/~sastry/pubs/PDFs%20of%20Pubs2000-2005/Publications%20of%20Postdocs/ShimDavid/ShimHierarchicalControl2000.pdf

[41]https://www.researchgate.net/publication/257133119_Robust_PID_Controller_Design_for_an_UAV_Flight_Control_System

[42] https://www.mdpi.com/2218-6581/13/6/83

[43] https://www.gemsys.ca/uav-magnetometers/

[44] https://skybrary.aero/articles/autorotation

[45] https://ardupilot.org/copter/docs/traditional-helicopter-autorotation-mode.html

[46] https://www.sae.org/standards/content/j2601_202005/

[47] https://www.magnet-schultz.com/en/valves-for-hydrogen-storage-and-fuel-cell-systems

[48] https://arc.aiaa.org/doi/10.2514/6.1999-4100

[49] https://ieeexplore.ieee.org/document/8516437

[50]https://www.faa.gov/sites/faa.gov/files/regulations_policies/handbooks_manuals/aviation/helicopter_flying_handbook/hfh_ch03.pdf

[51] https://www.faa.gov/sites/faa.gov/files/08_phak_ch6.pdf

[52] https://helicoptermaintenancemagazine.com/article/understanding-helicopter-automatic-flight-control-systems-afcs

[53]https://www.faa.gov/regulations_policies/rulemaking/committees/documents/media/Energy%20Supply%20Device%20ARC%20Recommendation%20Report.pdf

[54] https://www.sciencedirect.com/science/article/abs/pii/S0196890415007116

[55] https://www.mdpi.com/2079-9292/9/11/1889

Nomenclature:
A: Ampere
BoP: Balance of Plant
CAD: Computer Aided Design
CFD: Computational Fluid Dynamics
CFRP: Carbon Fiber Reinforced Polymer
CG: Center of Gravity
CNC: Computer Numerical Control
COPV: Composite Overwrapped Pressure Vessel
DOE: Department of Energy
ECU: Engine Control Unit
FC: Fuel Cell
Gpa: Giga Pascal
GPS: Global Positioning System
H2: Hydrogen
H2O: Water
HIGE: Hover In Ground Effect
HOGE: Hover On Ground Effect
HTC: High Temperature Cooling
HV: High Voltage
IMU: Inertial Measurement Unit
INS: Inertial Navigation System.
kg: Kilogramr per Hour
km/h: Kilo Meter per Hour
Ku: Gain applied to the x direction velocity error
Kv: Gain applied to the y direction velocity error Kilo wat
kW : Kilo wat

kW: Kilowatt
kWh: Kilo Watt Hour
LHV: Lower Heating Value
LTC: Low Temperature Cooling
LTC: Low temperature coolant
LV: Low Voltage
LVH: Lower heating value
m: Metre
MEA: Membrane Electrode Assembly’
Mpa: Mega Pascal
MSL: Mean Sea Level
MV: Medium Voltage
N: Newton
NASA: National Aeronautics and Space Administration
Nm: Newton Metre
O2: Oxygen
PCA: Pressure Control Analysis
PCA: Pressure Contour Analysis
PEM: Proton Exchange Membrane
PEMFC: Proton Exchange Membrane Fuel Cell
PID: Proportional Integral Derivative
PWM: Pulse Width Modulation
RFP: Request For Proposal
ROC: Rate of Climb
rpm: Rotation per minute
RT Linux: Real-Time Linux
RUAV: Rotorcraft-based Unmanned Aerial Vehicle.
SAE: Society of Automotive Engineers
SDC: System Design Constraints
SISO: Single Input Single Output
TFCM2s-B: Toyota Fuel Cell Module 2nd generation, Type B.

TKE: Turbulence Kinetic Energy
UART: Universal Asynchronous Receiver-Transmitter
UAV: Unmanned Aerial Vehicle
USD: United States Dollar
V: Voltage
Vbe: Best Endurance Velocity
Vclimb: Climb velocity
Vdescent: Descent velocity
VFS: Vertical Flight Society
VTOL: Vertical Take Off Landing
R: Propeller radius(m)=3.39m
N_b: Number of Blades = 3
ρ: Air Density (kg/m^3)=1.225 kg/m^3
ω:Rotational Speed(rad/s) =500rpm= $\frac{2\pi n}{t}$ =52.36 rad/s
V_∞: Axial Inflow Velocity=(Hover=0)
$c(r)$: Chord Distribution=0.18m
C_D:Drag Coefficient=0.023
$\dot{C}_L$: Lift Coefficient=1.46
α : Highest pitch angle of blade
r: Local radial position of the blade element (m)=400
V_t:Tangential Velocity (due to rotation)
dD: Differential Drag Force
V_a:Axial Velocity (including induced velocity)
Vrel: Resultant Relative Velocity
dL: Differential Lift Force

dT: Differential Thrust
Ttotal: Total Thrust
Qtotal: Total Torque
T: Thrust
τ: Torque
P: Power
Vnew: Induced Velocity
$(L/D)_e$: Lift to Drag Ratio
D: Max Cruise Speed
Pnet: Hydrogen Flow Rate and Consumption
Vbr: Velocity for Best Range

Table List:

Table- 1.7.3.i: Veloicty Transmission Efficiency
Table-2.4.i: Electrical specifications of motor [13]
Table- 3.1.2.6.i: Mass table of the main and tail rotor.
Table- 3.2.1.i: For 5kg of Hydrogen Tank. v
Table- 3.2.3.i: Key Fuel Cell Stack Parameters
Table- 3.2.10.2: Simulation Inputs and Parameters
Table-3.8.i: Input variables for the Airflow system.
Table-3.8.ii: Output variables for the Airflow system
Table-4.7.i: Performance Analysis
Table-5.1.i: Subsystem Estimated Cost Pie chart and weight distribution graph
Table – 7.3.3.i: System Component and Location in The Hawk.

Figure List:

Fig-1.6.i: Going flight mission segment.

Fig-1.6.ii: Returning flight mission segment

Fig-1.7.i: CL vs alpha curve

Fig-1.7.ii: Power and Fuel vs Velocity curve

Fig-1.7.iii: Range Performance vs Velocity curve

Fig-1.7.iv: Endurance performance vs velocity

Fig-1.7.1.i: Dimension.

Fig-1.7.1.ii: Isometric view.

Fig-1.7.1.iii: Inside view.

Fig-1.7.3.i: Aerodynamic power and Vehicle Power comparison for each segment.

Fig-1.7.4.i: Lift to Drag ratio vs Velocity

Fig- 2.2.i: Examples of conceptual VTOL aircraft that fulfill the dimensional requirements.

Fig-2.3.i: LTC cooling system showing that its perfectly functioning under 90°

Fig-2.4.i: EMRAX 268 motor integration with main and tail rotor.

Fig-2.5.i: Total Deformation under pressure

Fig-2.6.i: Von Mises Analysis on Cylinder

Fig-2.6.ii: (60+60 L) H2 tank and cross section.

Fig-3.1.1.i: Truss Type Aluminum Tubular Frame

Fig-3.1.1.1.i: Airframe static strain Chassis Simulation

Fig- 3.1.1.3.i: Static Displacement Analysis.

Fig- 3.1.2.1.i: Fully Articulated Main Rotor System

Fig- 3.1.2.1.ii: Tail rotor with actuator.

Fig- 3.1.2.2.i: Flapping

Fig- 3.1.2.2.ii: Lead Lag

Fig- 3.1.2.2.ii: Control Mechanism

Fig- 3.1.2.2.ii: Pitch

Fig- 3.1.2.3.i: Main rotor system dimension.

Fig- 3.1.2.3.ii: Tail rotor dimensions.

Fig- 3.1.2.4.i: Blade Structure.

Fig- 3.1.2.5.i: Reduction Gear.

Fig-3.2.i: TFCM2-B

Fig-3.2.ii: Toyota TFC-M2B Fuel Cell System CAD Model

Fig-3.2.iii: FC module

Fig-3.2.iv: PEMFC system for the Hawk

Fig-3.2.v: PEMFC architecture

Fig- 3.2.6.1: Humidification and Water Management System CAD model.

Fig- 3.2.7.i: Cooling System, Air Flow and Fuel Low Integration in The Fuel Cell (CAD model)

Fig- 3.2.10.1.i: Architecture and Design Rationale
Fig-3.2.10.3.i: Simulation output
Fig-3.3.i: LTC System
Fig-3.5.i Air Intake System
Fig-3.6.i: Cooling System
Fig–3.6.ii: Counter Flow Fin Radiator Setup
Fig- 3.6.iii: Cooling system and air intake system integration in the mainframe.
Fig-3.7.i: H2 vs. Current graph.
Fig-3.7.ii: Hydrogen Delivery Valve.
Fig-3.7.iii: Pressure distribution over valve
Fig-3.7.iv: Velocity Profile
Fig-4.1.i: Power vs Thrust
Fig-4.1.ii: Voltage vs Current
Fig-4.2.i: Pressure Control
Fig-4.2.ii: Velocity Streamline
Fig-4.3.i: TKE for R22
Fig-4.3.ii: Overall TKE
Fig-4.3.iii: TKE for Cabri
Fig-4.4.i: VS for R22
Fig-4.4.ii: Overall Velocity Streamline
Fig-4.4.iii: VS for Cabri
Fig-4.4.iv: VS for the Hawk
Fig-4.5.i: PCA for the R22.
Fig-4.5.ii: Overall PCA.
Fig-4.5.iii: PCA for the Cabri.
Fig - 4.5.iv: PCA for the Hawk.
Fig-5.2.i: Cabin material
Fig-5.2. ii: Landing Skid Material.
Fig-6.1.i: Fuel cell and Motor placement.
Fig-6.2. i: Truss Type Aluminum Tubular Frame
Fig–6.3.i: Cabin view
Fig-7.1. i: The architecture of proposed SISO multi-loop controllers [SISO]
Fig- 7.1.ii: Hierarchal flight control system.
Fig-7.3.i: Annotated Avionics Subsystem Diagram.